Applied Energy 301 (2021) 117455

Contents lists available at ScienceDirect

Applied Energy

journal homepage: www.elsevier.com/locate/apenergy

Combining sorption storage and electric heat pumps to foster integration of solar in buildings

Efstratios Tzinnis [a], Luca Baldini [b,*]

[a] ETH Zurich, 8092 Zurich, Switzerland
[b] Zurich University of Applied Sciences, 8401 Winterthur, Switzerland

HIGHLIGHTS

- Building integrated sorption storage with air-source heat pump and photovoltaics.
- Winter electricity demand and CO_2 emission reductions of up to 41%.
- Dynamic building simulations for optimal component sizing and system performance.
- Novel grey box model of liquid sorption storage.

ARTICLE INFO

Keywords:
Liquid sorption storage
Long-term thermal energy storage
Seasonal energy storage
Energy flexibility
Power to heat
PV integration

ABSTRACT

This article presents a numerical study on the building integration of a liquid sorption storage combined with an air-source electric heat pump. The double staging of the sorption storage (i.e. a chemical heat pump) and an electric heat pump leads to significant electricity demand and CO_2 emission reductions. Further, it provides an effective coupling between the heat demand of the building and the electricity supply, allowing for optimal integration of solar energy using photovoltaics. For the buildings analyzed, an autarky level of up to 83% is achieved. Winter electricity demand and emission reductions respectively reached values of up to 41%.

The storage integration was studied performing dynamic building simulations. The simulation model for the liquid sorption storage was based on a grey box approach. This features a simple analytical model being tuned to match with performance data available from experiments conducted on a lab scale test rig.

The presented integration of a compact seasonal thermal energy storage at the building scale represents a promising approach for a grid compliant integration of renewable energy, significantly reducing electricity demand peaks and related CO_2 emissions in winter.

1. Introduction

In the course of the Paris agreement, signed by many countries [1], GHG emissions need to be reduced in order to limit global warming. This requires, among other directives, substitution of fossil fuels with renewable energy sources. In many regions of Europe with an expressed climatic variance between seasons and rather cold winters, the largest energy demand in the building sector is in winter, for space heating and domestic hot water production. Available renewable, especially solar energy during winter is not sufficient to fully supply the energy demand. This creates a need for seasonal energy storage as sufficiently high imports of renewable energy from neighboring countries is unlikely, with everyone sharing the same goal of GHG emission reduction.

In buildings, electrification of heat generation plays a very important and ever-increasing role in substituting fossil fuels. For this reason, heat pumps gain importance, as can be observed by its increasing market share, with double-digit growth for the fourth consecutive year in Europe [2]. Through these heat pumps, a sectoral coupling (power to heat) is achieved, enabling building thermal management to play a very important role for the integration of renewables and stabilization of the electricity grid. Buildings with integrated thermal storage can either increase the share of integrated on-site renewables or provide energy flexibility to the electricity grid. While short-term flexibility can be provided with state-of-the-art sensible water storages or available thermal mass of the buildings, seasonal energy flexibility can be provided through integration of seasonal thermal energy storage. The latter is of greatest importance to increase electric efficiency in winter and is in

* Corresponding author.
E-mail addresses: efstratios.tzinnis@alumni.ethz.ch (E. Tzinnis), luca.baldini@zhaw.ch (L. Baldini).

https://doi.org/10.1016/j.apenergy.2021.117455
Received 15 March 2021; Received in revised form 12 July 2021; Accepted 15 July 2021
Available online 29 July 2021

Nomenclature

Abbreviations

COP	coefficient of performance
DHW	domestic hot water
GHG	greenhouse gas emissions
HP	heat pump
SAHP	solar-assisted heat pump
DX-SAHP	direct expansion solar-assisted heat pump
PV/T	hybrid photovoltaic solar thermal collector
HTF	heat transfer fluid
HX	heat exchanger
HMX	heat and mass heat exchanger
MF	heat pump modulation factor
PV	photovoltaics
SFH	single family house
SH	space heating
SR	sorption reactor

Latin letters

c_p	specific heat capacity [kJ•kg^{-1}•K^{-1}]
h	specific enthalpy [kJ/kg]
m	mass flow rate [g/min] or [kg/h]
N	number of nodes
p	pressure [kPa]
P	power [W] or [kW]
Q	heat transfer rate [W] or [kW]
T	temperature [°C]
UA	Overall heat transfer rate [W/K]

Greek letters

Δ	difference
η_{is}	heat pump isentropic efficiency
θ	temperature [°C]
ω	mass concentration [kg NaOH/kg solution]

Subscripts

A	absorber
C	condenser
D	desorber
E	evaporator
i	node number in discretized model
in	inlet to sorption reactor
out	outlet from sorption reactor
pr.	after preheating section
s	sorbent solution
sat.	at saturation pressure/temperature
x	input variable

the focus of this research. Liquid sorption storage is considered a seasonal thermal energy storage which allows direct building integration. To this end, the sorption storage is combined with a compression heat pump to provide necessary heat source and sink respectively as laid out in [3]. The sorption process acts as a chemical heat pump that, together with a compression heat pump, represents a hybrid double-stage heat pump. Due to the extra temperature lift provided by the sorption process when discharging, the compression heat pump operates with low temperature lift and thus high electric efficiency. Renewable energy harvested in summer and provided by on-site PV or excess electricity from the grid is used to charge the sorption storage in summer and to discharge it in winter with little electricity input. This way, an effective seasonal load-shift is achieved.

In contrast to the study presented in [3], where a strongly simplified sorption storage model was used along with a monthly resolution of weather data and space heating loads, this article provides a much more detailed analysis. Featuring a grey box model of the sorption storage (calibrated with experimental data), a dynamic building simulation is used to evaluate the gain in winter COP of the heat pump when combining it with a sorption storage. The efficiency gain in winter is equivalent to the provided seasonal load shift or seasonal flexibility offered to the grid. In this study, the integration of on-site PV with building integrated sorption storage for a single-family home is looked at specifically.

1.1. Building integrated sorption storage

Sorption processes enable long-term thermal energy with low thermal losses and relatively high volumetric energy densities when compared to regular sensible water storages. This makes them attractive to the building application for reaching high solar fractions through seasonal load shifting. For this reason, integration of sorption storage for building space heating and hot water production has been a promising area of research, focusing on novel sorption materials, components and systems [4–14]. Examples of experimental testing of sorption storage under realistic building application conditions are presented in [15] or [16]. In these studies, realistic but static temperature boundary conditions are applied for testing, allowing only for a first performance estimation. However, little dynamic performance predictions of a building integrated sorption storage have been undertaken. Even though many performance estimations of sorption storages are dedicated to building applications, there are only few studies addressing s fully integrated sorption storage systems in buildings.

Some early developments of sorption storages for buildings, s in the frame of the IEA SHC Task 32, featured building system simulations with experimentally validated theoretical models [17–19]. At this state, there were still many open prevailing questions regarding sorption storage application, including suitable materials and reactor designs, leading to successive IEA collaboration programs in this area, such as the IEA SHC Tasks 42 and 58 and jointly the ECES Annexes 29 and 33. In the frame of the EU funded project COMTES, [20] and [21] presented further results of building integrated storages applying dynamic building simulations. Adapted from the prototype developed in the EU funded project MODESTORE, a novel solid sorption fixed bed reactor experiment and building system simulation is presented in [22], identifying higher storage density and thus solar fraction achieved when using sorption storage instead of regular sensible water storage. In [23], another building integration of a solid sorption (strontium bromide) reactor is presented without description of the particular storage model used or an experimental counterpart to the simulations. In [24], a generalized approach considers the climatic boundary conditions, along with the building's heating demand and required space heating supply temperatures, to evaluate the potential of building integrated sorption storages under different climates in different geographical locations. This represents a crucial step in defining realistic operational boundary condition for sorption storages. In this approach, the system side comprising ground heat exchangers, solar collectors, buffer tanks, etc…, is not considered in detail but represented by static operating temperatures only. As such, the dynamic nature and physical inter-component coupling is not being considered.

Besides space heating application, implementation of sorption storage for space cooling purpose has been demonstrated by [25], presenting experimental testing and system evaluation of a sorption storage reactor. Different from a sorption chiller with a continuous cycle, the presented approach relies on a discontinuous storage cycle with direct solar charging of a phase change material during the day to then run the

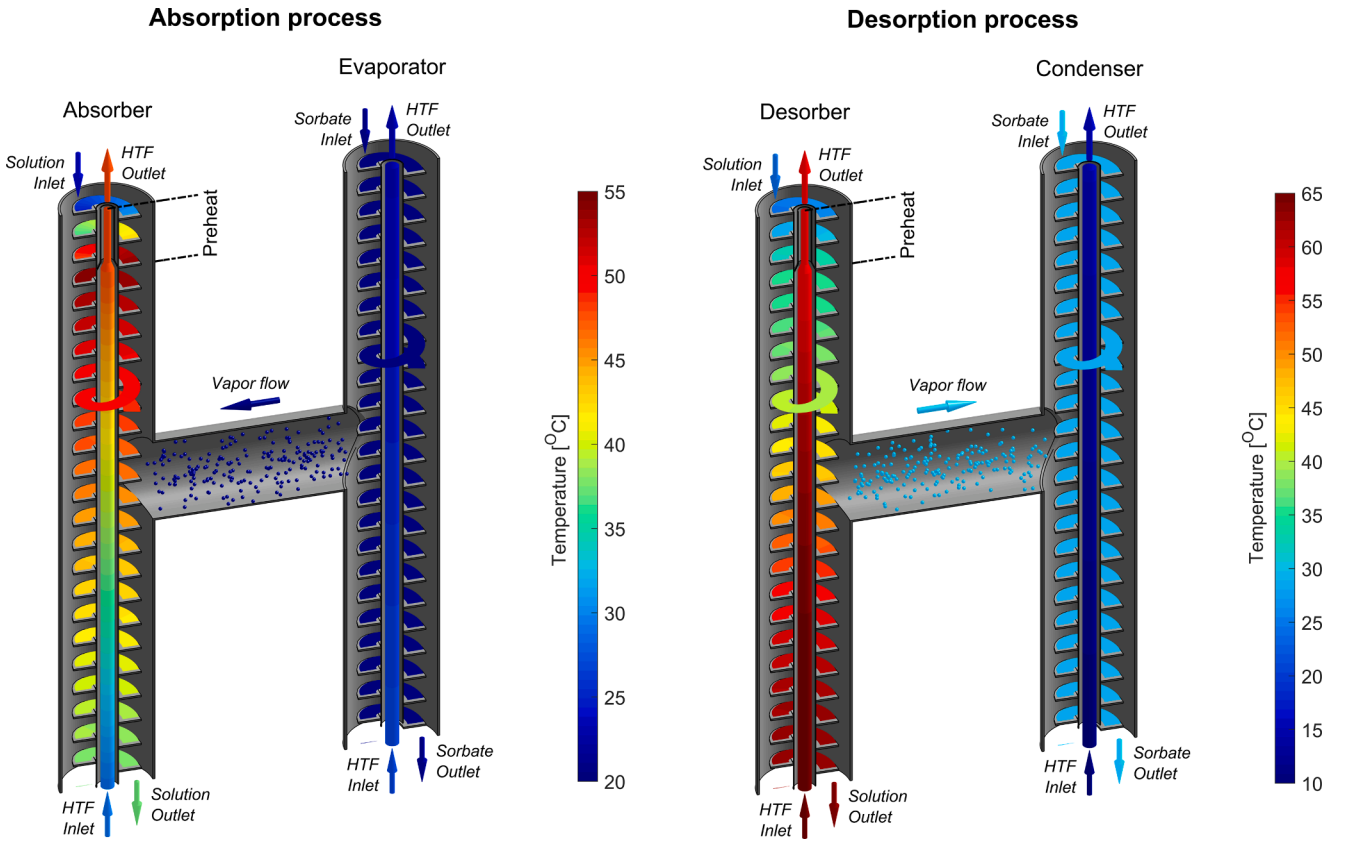

Fig. 1. Sorption reactor HMX operation in section view operating in discharging mode (left) and charging mode (right).

absorption storage for cold generation during the night. This requires an additional cold storage to shift the created cooling potential to the day when it is needed.

The bulk part of reported sorption enhanced building energy systems are purely thermal energy systems, combining sorption storage with solar collectors (acting as high temperature heat sources) and ambient air or soil (acting as low temperature heat sources and sinks). Sorption and sorption storage processes are also applied in the building context in combination with electric heat sources, such as compression heat pumps or direct electric heaters, offering energy flexibility to the electricity grid. An adsorption heat pump combined with a sensible water storage (to maximize available storage capacity) is presented in [26], and evaluated for space heating applications, assuming simplified boundary conditions by sampling different part load operation points. The presented setup aims to provide energy flexibility through energy storage and efficient discharging while accepting higher electricity demand during off-peak charging of the storage tank to high temperatures around 100 °C. The combination of a compression heat pump with an open sorption storage process for space heating is presented in [27], where the heat pump is used only for charging and the required temperature lift in discharging is entirely provided by the sorption storage. Additionally, this offers some energy flexibility as charging of the storage can be done during off peak times and discharging is taking place with little electricity demand. In [28], energy flexibility of a building featuring different thermal energy storages, including sorption storage is being quantified. The building side is represented by a simplified resistance–capacitance model, capturing more realistic building dynamics. The timescale considered for storage is 24 h, which is unable to evaluate longer-term storage capabilities of sorption storage. This is in line with other studies evaluating energy flexibility in the building context, typically focusing on short-term storage exclusively [29,30].

All systems investigated are fixed bed solid sorption processes (open and closed cycle), excluding the closed cycle, agitated liquid (sodium hydroxide) reactor discussed in [21]. Based on further developments of this concept [31], a new grey box model is developed and presented in this article. This model is used as a basis for a full, dynamic building simulation allowing for a realistic assessment of a building integrated liquid sorption storage. Another grey box modelling approach applied to sorption storage is presented in [32], applying neural networks trained with simulation results from a dynamic, spatially resolved numerical storage model.

1.2. Hybrid sorption compression systems

Beyond the storage application, coupling of sorption and vapor compression cycles is used for domestic as well as industrial heating and cooling. Similar to the aim of this study, this hybrid approach is motivated by its potential to either reduce the electricity demand of the vapor compressions cycle, to achieve higher over-all temperature lifts or to allow for flexible operation with strongly varying loads [33]. The hybrid concept of so called sorption-compression heat pumps dates back to more than 100 years, with a conceptual and historic review on these hybrid approaches presented in [34]. A more recent review and classification of different combinations of sorption and vapor compression cycles for cooling is given in [35] and for heating in [36]. A recent investigation in a cascading coupling for space cooling application is presented in [37] and a parallel integration for space heating and cooling in [38].

The current study also investigates a cascading coupling of the sorption and the vapor compression cycle with the aim of reducing the temperature lift to be provided by the electric heat pump. But unlike most studies presenting continuous hybrid sorption / vapor compression cycles, this study focuses on the seasonal energy storage through a discontinuous sorption process (two half cycles) with a temporally shifted charging and discharging. With this, the focus is on the generation of the space heating in winter when little solar energy is available

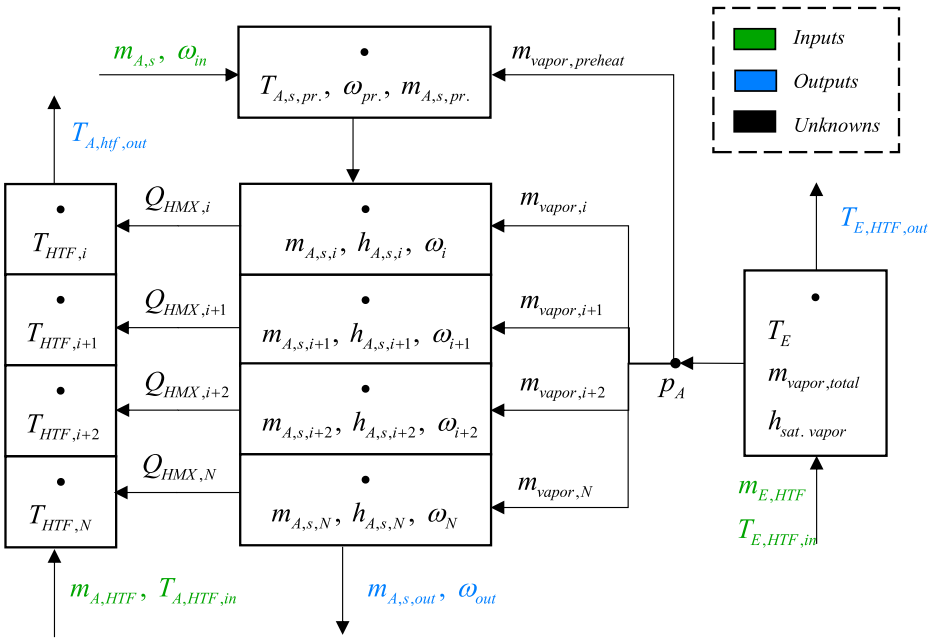

Fig. 2. Schematic of spatially discretized, 1D, steady state model.

rather than on space cooling, coinciding with largest solar intensities in summer.

1.3. Research gap

Literature research of building integrated sorption storage showed that most application cases focus on purely thermal energy system designs. The ongoing electrification in the building sector and the increasing need for energy flexibility is incentivizing thermo-electric building energy systems e.g. the combination of electric heat pumps with thermal storages. In this domain, mainly studies featuring state-of-the-art sensible storages are available and little research is done yet in combination with sorption storage. Coupled sorption and vapor compression cycles investigated are more strongly focusing on the solar cooling application using continuous cycles rather than on the heating application with discontinuous storage cycles. Further, studies considering sorption storage, mostly rely on short-term rather than on long-term storage capabilities and consequently offered seasonal energy flexibility. For this reason, investigation of seasonal energy flexibility and electric load shifting for improvement of winter performance of building integrated heat pumps is considered little explored yet.

Besides offering energy flexibility to the electricity grid through integration of thermal storage, the latter enables the integration of on-site PV electricity production. This is particularly interesting judging from the market figures, PV systems are gradually displacing solar thermal collectors [39] and their building integration will become an important factor in the future of renewable electricity supply. This research uniquely addresses the potential of on-site PV integration in combination with a building integrated liquid sorption storage.

There are only few studies evaluating current developments of sorption storages for the building application using full, dynamic building simulations. Due to the strong dependency of sorption performance on heating loads and various operating temperatures, a realistic evaluation is only possible through dynamic building simulations modelling all relevant energy system components.

The numerical models used to represent the sorption storage are often strongly simplified because of otherwise excessive computational costs. Only one example of a sorption storage meta-model using neural networks was found in literature allowing for fast evaluation as required in dynamic building simulations. Similarly, this research presents a data-fitted physical model as a novel and suitable approach to realistically capture storage performance under different operating conditions. Because of the continuous liquid sorption process a quasi-steady state model is sufficient to be used in the building simulation. This is in strong contrast to the sorption storages presented in literature, all relying on either open or closed but fixed bed solid sorption processes, asking for dynamic representation of the state-of-charge of the storage. Thus, providing more insights and results from evaluation of liquid sorption storage in the building context is valuable, allowing for better performance comparison with solid sorption storage systems forming the bulk of sorption storage systems investigated.

2. Material and methods

The basic working principle of the liquid sorption storage addressed here is present in the heat and mass exchanger (HMX) shown in Fig. 1. This HMX, follows the design introduced in [31], and is operated either in a charging or in discharging mode. Depending on the mode, it hosts either the desorber and condenser or the absorber and evaporator. The HMX thus features two heat exchanger coils embedded in a common housing. Inside the inner tube of the coils, heat transfer fluid (HTF) is transported while on the outside, along the spiral fins, liquid sorbent or water trickles down. As sorption couple, aqueous sodium hydroxide (sorbent) is considered together with water (sorbate).

In charging mode, renewable heat is used in the desorber to evaporate water vapor from a diluted sorbent solution. The water vapor passing to the other side of the HMX condenses on the condenser coil, rejecting the latent heat to a suitable low temperature heat sink. When discharging, the process is reversed. Water vapor is generated in the evaporator using a renewable low temperature heat source, passes to the other side of the HMX where it is absorbed by the highly concentrated sorbent solution and heat is released. The released heat can be used for space heating or domestic hot water production. One particularity, significant only during discharging, is the preheating of the sorbent solution. This takes place in the preheating section at the top of the absorber (marked as Preheat in Fig. 1). There, the sorbent solution entering at room temperature absorbs water vapor and heats up before releasing heat to the HTF. For this reason, the spiral fins of the heat exchanger in this location are decoupled from the inner tube carrying the HTF.

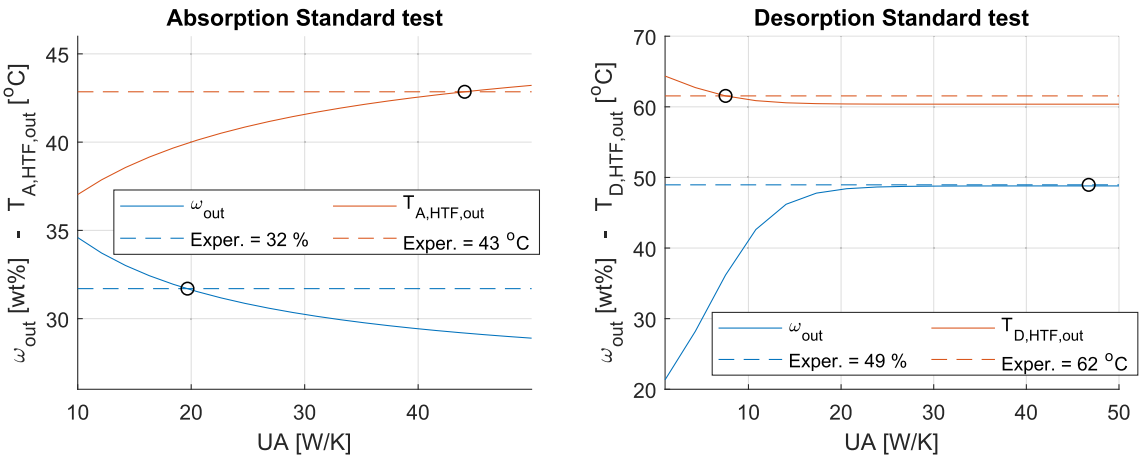

Fig. 3. Example of UA value contradictions in standard absorption (left) and desorption (right) tests.

2.1. Sorption reactor HMX model

2.1.1. Basic steady state equilibrium model

The basis for the modelling of the sorption storage process is a 1D, steady-state, equilibrium model, based on mass end energy balance formulations discretized in space. This model yields concentration and temperature profiles along the HMX of the storage, which can be used to determine its performance. The thermophysical properties of the considered sorbent as an aqueous sodium hydroxide solution were calculated based on the work presented in [40]. The one dimensional schematic of the model's operation during absorption is illustrated as an example in Fig. 2, and the mathematical model for the absorption process is briefly described in Eqs. (1)–(12). The vapor transport is considered in Eq. (10) and the associated pressure drop (ΔP) between the two chambers in Eq. (1) was taken to be 0.0554 kPa as suggested by the experimental data from [31]. The desorption process is represented by the same set of equations but with opposite signs, describing heat transfer from HTF to the sorbent solution and vapor transport out of the solution in the desorber

$$p_A = p_{saturated,vapor}(T_E) - \Delta P \quad \text{Vapor pressure} \tag{1}$$

2.1.1.1. Preheating section

$$T_{A,s,pr.} = f_{preheat,Abs}(T_E) \quad \text{Solution temperature after preheating} \tag{2}$$

$$\omega_{pr.} = \omega_{function}\left(p_A, T_{A,s,pr.}\right) \quad \text{Solution concentration after preheating} \tag{3}$$

$$\mathrm{m}_{A,s,pr.} = \frac{\omega_{in}}{\omega_{pr.}} \cdot m_{A,s} \quad \text{Solution flowrate after preheating} \tag{4}$$

2.1.1.2. Absorber/Desorber HMX

$$m_{A,s,i+1} = m_{A,s,i} + m_{vapor,i+1} \quad \text{Mass balance of the solution} \tag{5}$$

$$m_{A,s,i+1} \cdot \omega_{i+1} = m_{A,s,i} \cdot \omega_i \quad \text{NaOH balance} \tag{6}$$

$$Q_{HMX,i+1} = -m_{A,s,i+1} \cdot h_{A,s}(p_A, \omega_{i+1}) + m_{A,s,i} \cdot h_{A,s}(p_A, \omega_i) + m_{vapor,i+1} \cdot h(p_A)_{vapor}^{saturated} \quad \text{Energy balance of solution} \tag{7}$$

$$Q_{HMX,i+1} = m_{A,HTF} \cdot c_p \cdot \left(T_{A,HTF,i} - T_{A,HTF,i+1}\right) \quad \text{HTF energy balance} \tag{8}$$

$$Q_{HMX,i} = \frac{UA_A}{N_{nodes}} \cdot \left[T_{solution}(p_A, \omega_i) - T_{A,HTF,i}\right] \quad \text{Heat transfer : Sorbent→HTF} \tag{9}$$

2.1.1.3. Evaporator/Condenser HMX

$$m_{vapor,total} = m_{A,s,out} - m_{A,s} \quad \text{Vapor mass balance} \tag{10}$$

$$m_{vapor,total} \cdot \Delta h_{l \to g}(T_E) = m_{E,HTF} \cdot c_{p,HTF} \cdot (T_{E,HTF,in} - T_{E,HTF,out}) \quad \text{Heat transfer : Sorbate → HTF} \tag{11}$$

$$ln\frac{T_{E,HTF,in} - T_E}{T_{E,HTF,out} - T_E} = \frac{UA_E}{m_{E,HTF} \cdot c_p} \quad \text{LMTD in evaporator} \tag{12}$$

2.1.2. Experimental dataset/model fitting

Extensive measurements have been performed on the available experimental storage facility at Empa, presented in [31]. This measurement data was used together with the basic model to build a representative grey box model of the sorption storage.

Measurement data is available for the charging and discharging modes, for both, the absorber/desorber and evaporator/condenser. In the measurements various temperatures, volumetric flow rates and sorbent concentrations were monitored.

In the modelling process, first the preheat section is addressed. Two polynomial functions are established (Eq. (2)) to correlate the evaporator/condenser temperature data with the solution inlet temperature data to the HMX. The reason for this approach is the lack of thermophysical data in the literature describing the transition of sodium lye from an unsaturated state (storage tanks) to saturated vapor pressure conditions inside the absorber/desorber chamber.

Second, the actual HMX in the absorber/evaporator chamber is addressed with 50 nodes discretization as shown in Eqs. (5)–(9). Since the UA value of the HMX is a necessary input parameter, UA values were evaluated such that measurement and simulation are in good agreement. Contradictory results for the absorber/desorber chamber were observed as different UA values satisfy the measured heat transfer fluid outlet temperature and solution outlet concentration from the absorber/desorber respectively. Examples for the standard absorption and desorption tests, according to [31], are given in Fig. 3 below. In the standard test for absorption, as well as for desorption, a UA value of 45 W/K confirms the measured outlet heat transfer fluid temperature (red curve) and a value of 19 W/K confirms the outlet solution concentration (blue curve) as illustrated in Fig. 3 below.

This divergence regarding UA values can be explained with the ideal modelling of the process not being able to capture heat losses to the environment, along with unsaturated vapor pressure conditions occurring along the HMX. Moreover, in this study, the UA value is assumed to be constant along the height of the chamber while in reality it is expected to vary as the solution flowrate on the fins increases in absorption while water vapor is absorbed. Similarly, it decreases in desorption while water vapor is desorbed. For this reason, the mathematical model

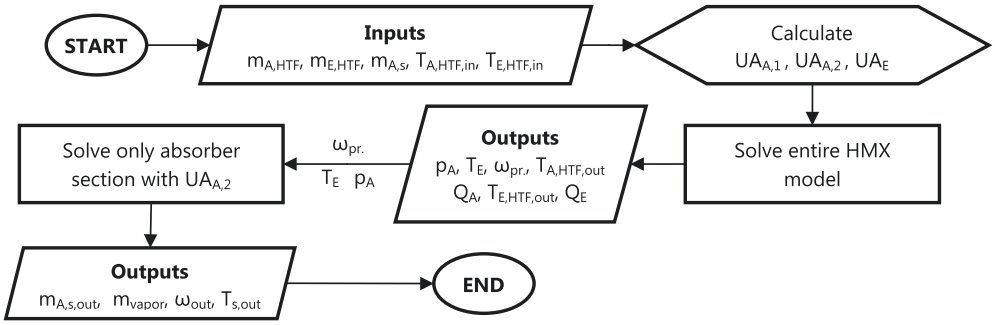

Fig. 4. Grey-box model algorithm flowchart: Example for absorption.

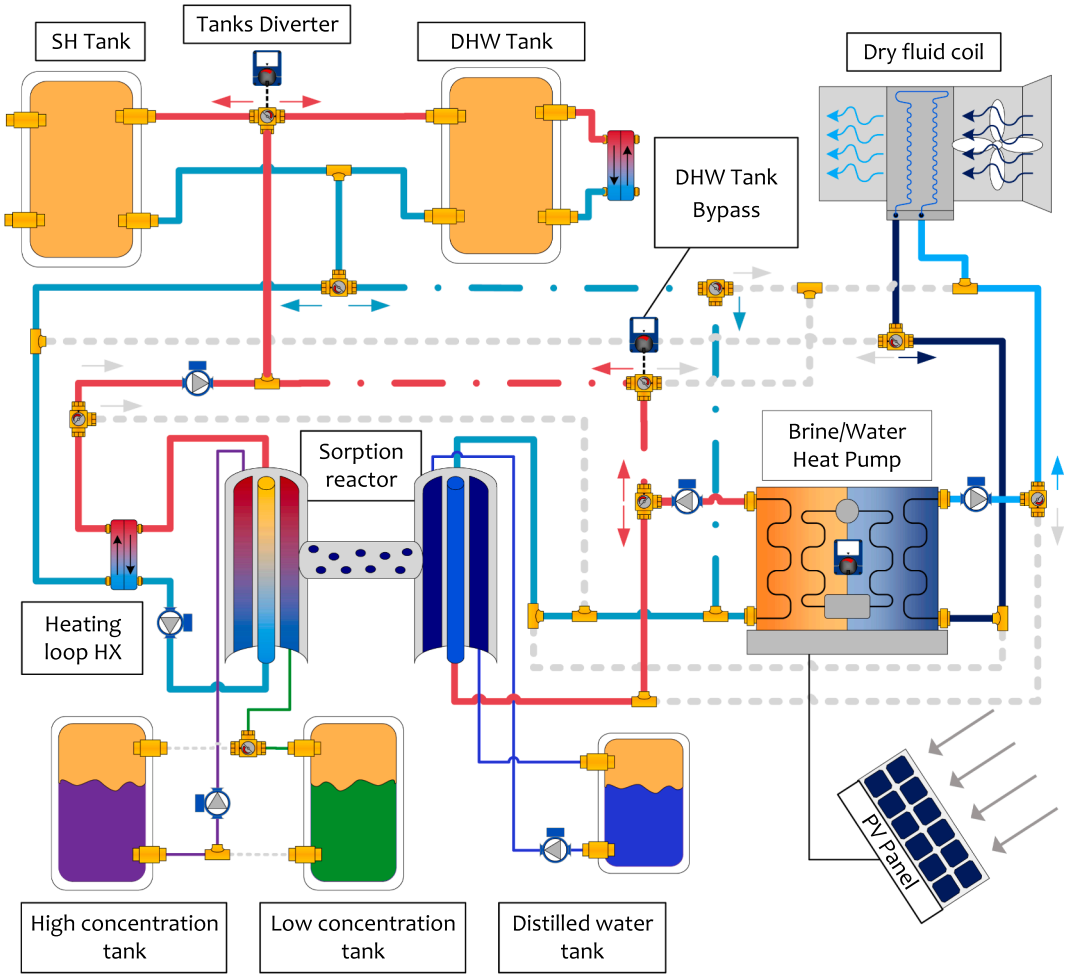

Fig. 5. Energy system schematic during winter (discharging). The dash-dot lines represent the operation of the system without the sorption storage.

will be solved twice to obtain more accurate results. The entire system of equations will thus be solved with the UA value calculated for the $T_{A/D,htf,out}$ (from now on referred to as $UA_{A,1}$) to obtain all outputs, except for the sorbent mass fraction ω_{out}. After this, the absorber/desorber equations will be solved again with the second UA value to calculate ω_{out} (from now on referred to as $UA_{A,2}$). For the evaporator/condenser, the UA_E/UA_C values were determined using the experimental data for the evaporator/condenser chamber.

A further step in the grey box modelling was the extension of the operation range past the predefined experiments. The three UA values ($UA_{A,1}$ for $T_{A/D,htf,out}$, $UA_{A,2}$ for ω_{out} and UA in the evaporator/condenser vary considerably between the conducted experiments. For this reason, there was a necessity of establishing a method that estimates these changes based on the model inputs. To this end, the impact of each input parameter on the UA value was examined. Polynomial fits were used to obtain a continuous function describing this influence on the UA value for the different input parameters. An example of these functions can be found in Fig. A1 and Fig. A2 in the appendix for the HTF inlet temperature in the absorption chamber.

The polynomial fits are then used as partial functions $UA_x = f(x)$ to calculate the impact of input x on the UA value. The UA value in the standard test is then further used to calculate the imposed change of this input parameter on the UA value as $\Delta UA_x = UA_x - UA_{\text{Standard Test}}$. This impact is calculated for all inputs ($m_{A,htf}$, $m_{E,htf}$, $T_{A,htf,in}$, $m_{A,s}$ and $T_{E,htf,in}$

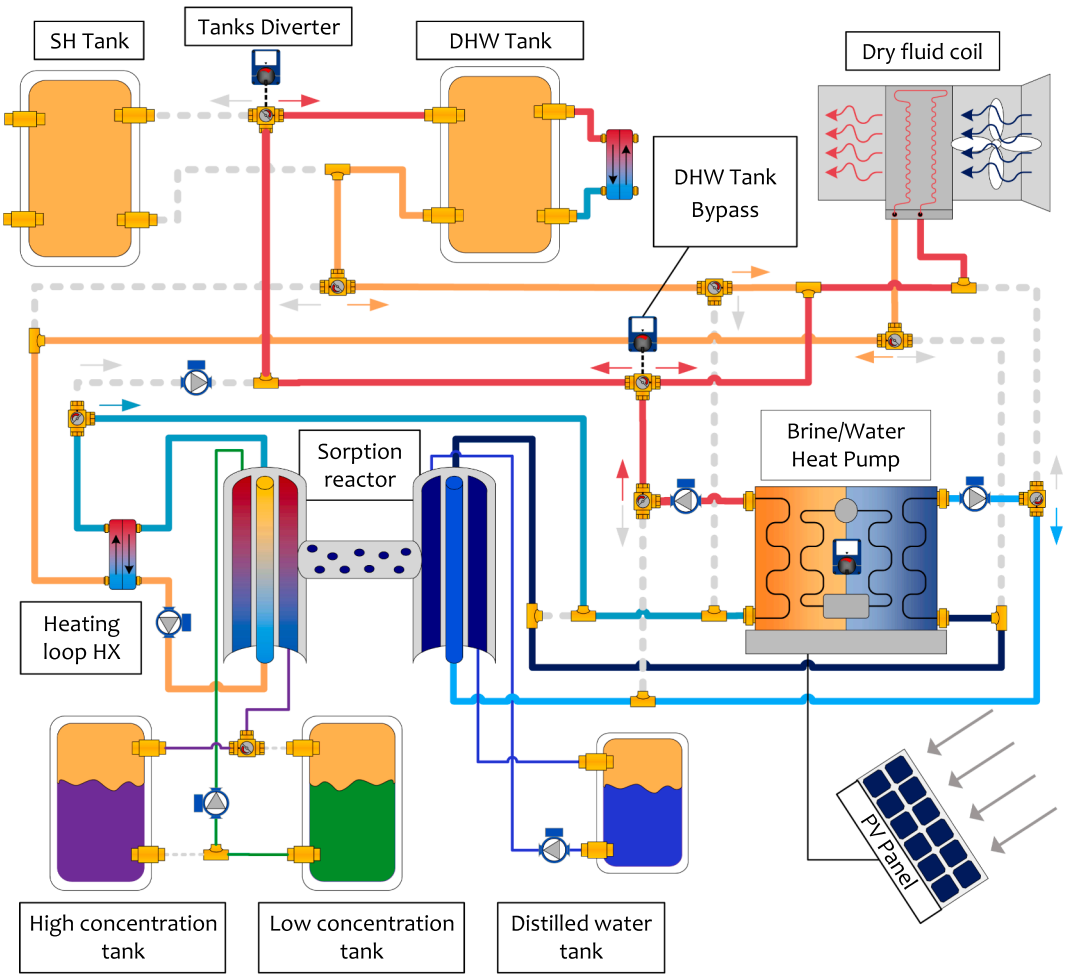

Fig. 6. Energy system schematic during summer (charging).

in absorption and $m_{D,htf}$, $m_{C,htf}$, $T_{D,htf,in}$ and $m_{D,s}$ in desorption) and a weighted average function is applied to combine all changes on the $UA_{S.T.}$ value as:

$$UA_{function} = UA_{\text{Standard Test}} + \frac{\sum \Delta UA_x \cdot w_x}{\sum w}, \text{ where } w_x = \frac{|\Delta UA_x|}{UA_{\text{Standard Test}}} \quad (13)$$

The comparison of the calculated UA values for every experiment and the performance of the UA function is presented in Fig. A3 and Fig. A4 in the appendix. Having the various UA functions established, the solving algorithm can now be implemented for any combination of different inputs. The flowchart in Fig. 4 gives the overview of the algorithm structure for the absorption process.

The developed grey box model was tested in the experiments' conditions and accurate performance predictions for most performance criteria were achieved as illustrated in Fig. A5 and Fig. A6 in the appendix. Predictions regarding thermal power (Q_A, Q_E and Q_D, Q_C) were the least reliable and hence included the largest prediction errors as the small divergences in temperatures were amplified in the thermal power calculations.

Apart from the UA function, inaccuracies, and the possibly unsaturated vapor conditions at some areas inside the HMX, the heat losses through the reactor's casing are mostly responsible for the divergence between the model and the experiment, despite the reactor being thermally insulated [31]. The heat losses were not modelled in this study and their impact on desorption is more significant than on absorption, as expected, due to the increased operating temperatures.

2.2. Building simulation

2.2.1. Energy system model

The system integration of the sorption storage together with an air-source heat pump (ASHP) was implemented similar to [3], but represented in greater detail. In contrast to the integration found there, a dynamic energy system simulation was performed using an hourly time resolution. The system implemented features space heating (SH) and domestic hot water (DHW) buffer storages, internal and external heat exchangers, circulation pumps and switching valves as shown in Fig. 5 and Fig. 6.

The discharging operation of the energy system during winter is illustrated in Fig. 5. The air-source heat pump provides the necessary heat to the evaporator of the sorption reactor (SR) while the absorber delivers the required heat to the hot water thermal storage tanks. The dash-dot lines represent the operation of the system without the sorption reactor, where the heat pump directly covers the buffer tank's demand. This operation mode is the reference scenario, with which the absorption storage system is compared. This mode is also employed when the high concentration sorbent solution tank is depleted, or the operation of the sorption reactor is not desired. The tank diverter selectively delivers hot water to the water storage tanks with the DHW tank having priority over the SH tank.

In the charging mode (Fig. 6) during summer, when no space heating load exists, the ASHP is directly coupled to the SR, with the HP evaporator connecting to the SR condenser and the HP condenser to the SR desorber. The evaporator of the ASHP matches the cooling demand of

the SR leading to a surplus of heat produced by the HP condenser. The surplus is rejected to the DHW tank and/or the ambient air via the dry air cooler. This splitting is controlled by the DHW Tank Bypass by a PID controlled diverter. It modulates the bypass stream towards the DHW Tank to make use of as much of the excess heat as possible. If the tank temperatures are not low enough to achieve the desired desorber inlet temperature, the mixed stream after the DHW tank bypass is passed through the dry fluid coil to further reduce its temperature.

The building integration has been studied for a single family home (SFH) located in Strasbourg, France according to a developed framework by the International Energy Agency [41,42]. Thereof, two scenarios, SFH45 and SFH100 with an average heating load of 45 and 100 kWh/(m^2 * a) respectively have been considered. In contrast to these references, the roof of the building was mirrored by 180° to maximize installable PV area. Hourly simulations were carried out for the Strasbourg climate in DesignBuilder [43]. Rooftop PV was integrated as an electric power supply profile, stemming from separate simulations with common PV panels carried out in Polysun [44]. Commercially available PV panels with a total area of 52.8 m^2 and a cumulated potential of 12 kW_p [45] were used in this study. In the IEA framework, the heat gains from electricity consumption are only partially considered. For simplicity, the heat gains were assumed to be equal to the total electricity load. Hourly varying electricity grid CO_2 emission intensities for Switzerland [46] were taken into account, as shown in Fig. A11 in the appendix. TRNSYS 17 [47] was used as the simulation environment for the building energy system modelling. To reduce the simulation time, the sorption reactor model was pre-solved under numerous combinations of the various input variables as described in chapter 2.1. The input variable space is multidimensional with multiple points for each input (e.g. $T_{A,htf,in}$ range is 20–54 °C with 2 K steps and $T_{E,htf,in}$ range is 10–40 °C with 2.5 K steps). The results were stored as tables and used as external files in TRNSYS by calling the built-in multi-dimensional linear interpolation routine during the dynamic simulations.

2.3. Building simulation/scenarios

To maximize the achievable solar fraction from the PV panels, heat generation is only allowed during the day, and the thermostats in the sensible water storage tanks monitor the temperature at the bottom. In this way, the entire water volume is heated up to cover the loads during night-time without the need of additional heat generation. The DHW thermostat is set to 50 °C in both building scenarios. On-demand DHW generation is assumed using an external heat exchanger (Figs. 5 and 6) to allow for low temperature operation while minimizing the risk of Legionella. The SH thermostat setpoint is 35 °C in the SFH45 and 50 °C in the SH100, based on the nominal supply temperatures of the space heating emission system (floor heating, radiators). The sizing of the tanks was determined with parametric tests to achieve enough thermal storage for the load coverage during night-time. The DHW tank is 200 l in both buildings and the SH tanks in SFH45 and SFH100 are 1800 l and 4000 l respectively.

The first step of the heat generation dimensioning is the selection of appropriate heat pumps. Modulating heat pumps are essential since they must match the SR evaporator demand during absorption. The SR absorber and evaporator power vary greatly depending on the inlet temperatures and are dependent on each other. Characteristic curves of the SR operation in absorption under various inlet temperatures can be found in Fig. A7 and Fig. A8 in the appendix. Additionally, the heat pump must be able to directly cover the building's heat demand in standalone operation. Heat pump capacity estimates can be based on the load duration curves. The latter represent the building's heating loads sorted by their magnitude over the course of the year. Choosing the heat pump to cover heating during a certain percentage of time determines the capacity necessary for installation. Indicatively, the total heating load (SH + DHW) for SFH45 is 2.5 kW, 2.8 kW and 3.3 kW at normalized load durations of 80%, 90% and 98% respectively. In the SFH100 the load reaches 4.4 kW, 5 kW and 5.9 kW for the same normalized load duration values. Therefore, two commercially available heat pumps with modulating capacity within the needed range were chosen: the Hoval Ultrasource comfort model T, sized at 8 kW for the SFH45 and at 13 kW for the SFH100 [48].

The power scaling of the developed sorption reactor model is assumed to be ideal and different scaling factors are applied to the absorber and desorber in discharging and charging operations respectively. In real life, this would translate into different numbers of parallel heat exchangers operated within the SR depending on charging and discharging mode. The modelled outlet temperatures and solution outlet concentration remain unaffected, but sorbent solution and HTF flowrates need to be adjusted by the scaling factor to match the power. In absorption mode, the setpoint temperature for the HTF at the SR evaporator's inlet is the key parameter for the performance of the sorption reactor as it affects the vapor pressure and consequently the HTF outlet temperature from the absorber, as well as the solution outlet concentration. The maximum allowable absorber outlet concentration ω_{out} is set to 35 wt%. This limitation is set to guarantee a minimum sorbent concentration difference during discharging and consequently a minimum volumetric energy density of the sorption storage. In the case of the SFH45, the SH tank charging requires temperatures of up to 40 °C while in the SFH100 case temperatures above 55 °C are necessary for SH. The appropriate setpoints for the SR evaporator inlet temperature were fixed at 25 °C and 35 °C respectively. For the DHW tank charging 35 °C is used even if there is simultaneous demand by the SH tank. Note that the 25 °C setpoint was chosen because of minimum ASHP condenser temperature requirements of most domestic heat pumps.

A low temperature lift is decisive for reducing the heat pump electricity consumption. For this reason, besides the commercial heat pumps, a modulating ideal heat pump with 10 kW nominal heating capacity (Eq. (15)) was additionally modelled in the SFH45 case with an SR evaporator inlet temperature setpoint of 19 °C. The COP of this ideal heat pump is calculated according to Eq. (14) below. The isentropic efficiency of 0.5 corresponds to the average isentropic efficiency over all inlet conditions of the Hoval ASHP (8 kW) at the nominal compressor operation. The use of the HP condenser inlet rather than the outlet temperature in Eq. (14) is a requirement of the TRNSYS solving algorithm. The inlet temperatures are calculated assuming a nominal temperature difference of 6 K and 4 K, which are applied across the condenser and evaporator respectively. The ideal HP COP (Eq. (14)) is used along with Eq. (16) to create an external file with a table containing $Q_{heating}$ and $P_{electric}$ under different modulation factors (MF) and condenser/evaporator inlet temperatures. During the simulations, HP condenser and evaporator outlet temperatures are not restricted by the 6 K and 4 K lifts in Eq. (15), as TRNSYS uses the user-given table with the heating and electric power to calculate the outlet temperatures based on the inlet conditions as shown in Eqs. (16) and (17). All the other settings in the new building case "SFH45 with Ideal HP" are the same as in the normal HP case.

$$COP_{Ideal\_HP} = 0.5 \cdot \frac{T_{Condenser,Inlet} + 6}{T_{Condenser,Inlet} + 6 - (T_{Evaporator,Inlet} - 4)} \tag{14}$$

$$Q_{heating} = 10kW \cdot MF,\ P_{electric} = \frac{Q_{heating}}{COP},\ \text{where MF} = [0...1] \tag{15}$$

$$T_{Condenser,outlet} = T_{Condenser,Inlet} + \frac{Q_{heating}}{m_{condenser} \cdot c_p} \tag{16}$$

$$T_{Evaporator,outlet} = T_{Evaporator,Inlet} - \frac{Q_{heating} - P_{electric}}{m_{evaporator} \cdot c_p} \tag{17}$$

The charging period is the bottleneck of the sorption storage system as already highlighted in [3]. For this reason, the solution flowrate during desorption should be as high as possible, while the solution flowrate in absorption should be just high enough to cover the heat

Table 1
Absorption operation settings.

Building	Scaling factor	Operation mode	SR $T_{E,htf,in}$ [°C]	SR $m_{A,HTF}$		SR $m_{E,HTF}$ –HP condenser flowrate	
				Setting [g/min]	Total [kg/h]	Setting [g/min]	Total [kg/h]
SFH45	35	SH	25	143	300.3	700	1470
		DHW	35				
SFH45 (ideal HP)	35	SH	19				
		DHW	35				
SFH100	50	SH	35		429		2100
		DHW	35				

Table 2
Desorption operation settings.

Building	Scaling factor	solution ω [wt.%]	SR $T_{C,HTF,in}$ [°C]	SR $m_{C,HTF}$ - HP Evaporator		SR $T_{D,HTF,in}$ [°C]	SR $m_{D,HTF}$ –HX cold side		HX hot side inlet setpoint [°C]	HP condenser – HX hot side flowrate [lt/h]	HP electricity consumption [kW]	Rejected heat [kW]
				flowrate setting [g/min]	Total flowrate [kg/h]		flowrate setting [g/min]	Total flowrate [kg/h]				
SFH45	56	31	10	405	1360	61.3	400	1344	61.4	1700	2.17	0.69
		32	10			60.0			61.4		2.06	0.60
		33	11			60.7			60.8		1.78	0.35
		34	12			61.2			61.4		1.52	0.14
SFH45		31	10		1360	61.3			61.6	1200	1.94	0.47
Ideal		32	10		1360	60.0			61.4		1.81	0.34
HP		33	11		1360	60.7			61.6		1.68	0.26
		34	12		1360	61.2			61.8		1.55	0.17
SFH100	87	31	10	402	2100	61.3		2088	61.6	2300	3.28	0.99
		32	11			61.7			62.0		2.91	0.67
		33	12			62.1			62.4		2.58	0.40
		34	12			61.2			61.5		2.47	0.33

demand of the building. Domestic heat pumps have a condenser outlet temperature limit of approximately 65–70 °C. Moreover, the sorbent solution must be regenerated to 50 wt% for the winter period. With these constraints, the developed desorption model was solved to obtain look-up tables with the required inlet HTF temperature to the desorber for different inlet solution concentrations and HTF inlet temperatures in the SR condenser. It was found that the maximum solution flowrate that can be regenerated (under the 65–70 °C limitation and at a power scaling factor of 1) is 6 g/min in all building cases. Characteristic curves for the desorption operation can be found in Fig. A9 and Fig. A10 in the appendix. Finally, the solution flowrate at a power scaling factor of 1 in absorption was set to 4 g/min in all building cases.

The power scaling factors can now be configured based on these settings. In absorption, a factor of 35 is used in the SFH45 cases and 50 in the SFH100 case. In desorption, the maximum possible scaling factors are used for increased charging speed; 56 in SFH45 and 87 in SFH100. The smaller scaling in discharging would result in parts of the heat exchangers inside the SR not being used.

The optimum HTF flowrates settings for a power scaling factor of 1 in absorption were determined after parametric tests at 143 g/min in the absorber and 700 g/min for the evaporator. As a rule of thumb, the evaporator HTF should have a large flowrate to maintain a high evaporator temperature, while the absorber should be fed with small flowrates to achieve a high enough outlet temperature. The return temperature from the space heating loop (absorber inlet temperatures) should be low in order to achieve low outlet sorbent concentrations and thus high volumetric energy density of the storage. Fig. A7 through Fig. A10 in the appendix are created for these settings and a normalized solution flowrate of 4 g/min. The discussed settings during absorption operation are summarized in Table 1.

The desorption process was optimized offline by running parametric tests on the various inputs. The coupling between the heat pump, the heating loop HX and the sorption reactor was examined and the settings which achieved the minimum electric consumption by the heat pump were used in the simulation. After this optimization, the only input variable is the solution concentration in the low concentration sorbent tank. TRNSYS performed linear interpolation on external files to retrieve the desorption settings. These user-given look-up tables for the SFH45 with the normal and the ideal HP as well as the SFH100 are presented in Table 2.

The last two components of the energy system are the heating loop heat exchanger and the dry fluid coil. The heat exchanger is mainly used to decouple the flowrates between the desorber and the heat pump in charging mode to have more flexibility. Additionally, it keeps the heat transfer fluid inside the SR clean and decoupled from the heating delivery system as hot water tanks often suffer from corrosion and salts accumulation. A flat plate heat exchanger was selected with an overall heat transfer coefficient of 120 kW/K achieving effectiveness above 98% effectiveness in absorption and above 92% in desorption at flowrate settings, given in Table 1 and Table 2.

The electricity consumption of the dry fluid coil is not considered in this study due to the lack of available commercial data on the operation of dry fluid coils in heating mode during winter. The absorption storage system is compared to the reference system using the same brine/water heat pump (Hoval comfort T series) combined with the same dry fluid cooler to source heat from the ambient air. For this reason, during winter, the coil electricity consumption in both systems (reference and absorption storage) is similar and the comparative results between the absorption storage and the reference system are hence expected to remain unaffected by the exclusion of the dry fluid coil electricity consumption.

Pumping energy is not considered in this study. The circulation pumps in both systems operate under similar conditions as the heating loop between the tanks and the heat producer remains almost the same. The only difference in the absorption system is the additional circulation pumps for the HTF in the HMX, but their electricity consumption is

Table 3
Available solution mass at 50 wt% and absorption periods at different PV thresholds.

SFH45			SFH45 with Ideal HP			SFH100		
$PV_{threshold}$	Sol. mass @ 50 wt% [tons]	Absorption period	$PV_{threshold}$	Sol. mass @ 50 wt% [tons]	Absorption period	$PV_{threshold}$	Sol. mass @ 50 wt% [tons]	Absorption period
0.0	16.1	10 Oct–26 Apr	0.0	20.1	10 Oct–26 Apr	0.0	34.3	16 Nov–16 Mar
0.3	16.1		0.2	20.1		0.4	32.0	20 Nov–12 Mar
0.6	16.1		0.5	20.1		0.7	29.7	24 Nov–08 Mar
0.9	16.1		0.7	20.1		1.1	27.4	28 Nov–04 Mar
1.2	16.1		0.9	20.1		1.4	25.6	01 Dec–01 Mar
1.6	16.1		1.2	19.2	22 Oct–14 Apr	1.8	23.3	05 Dec–25 Feb
1.9	15.6	18 Oct–18 Apr	1.4	18.3	30 Oct–06 Apr	2.1	22.2	07 Dec–23 Feb
2.2	14.6	27 Oct–09 Apr	1.6	17.6	04 Nov–01 Apr	2.5	20.5	10 Dec–20 Feb
Full-time	16.6	10 Oct–26 Apr	Full-time	20.6	10 Oct–26 Apr	Full-time	55.8	29 Sep–03 May

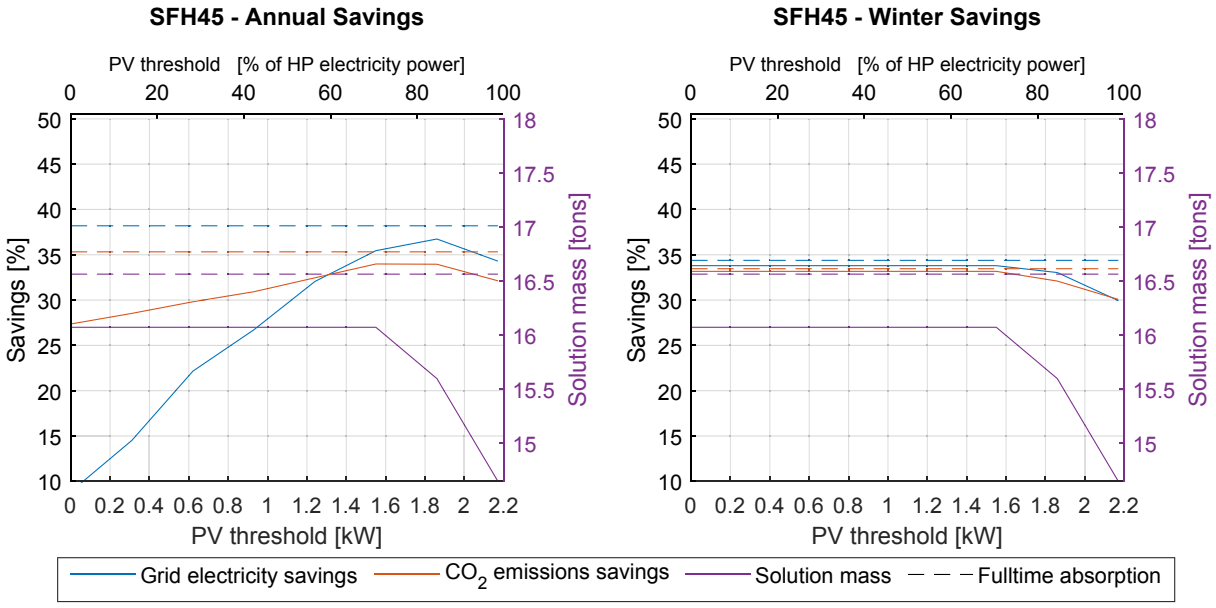

Fig. 7. SFH45 with real HP annual (left) and winter (right) grid electricity and CO_2 emission savings compared to reference system.

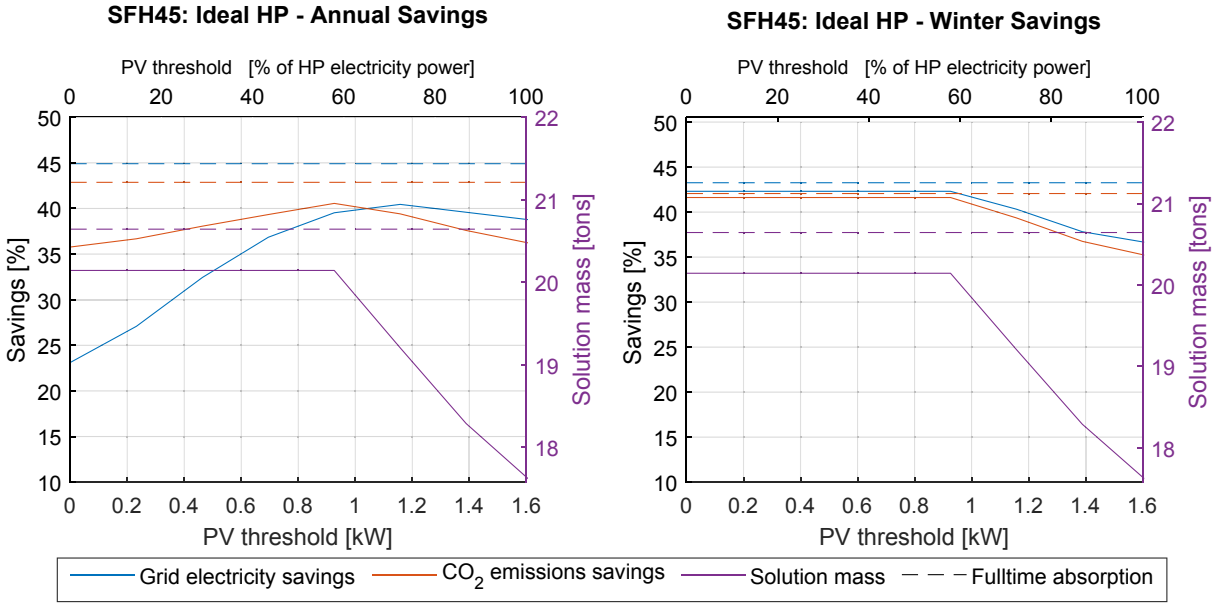

Fig. 8. SFH45 with ideal HP annual (left) and winter (right) grid electricity and CO_2 emission savings compared to reference system.

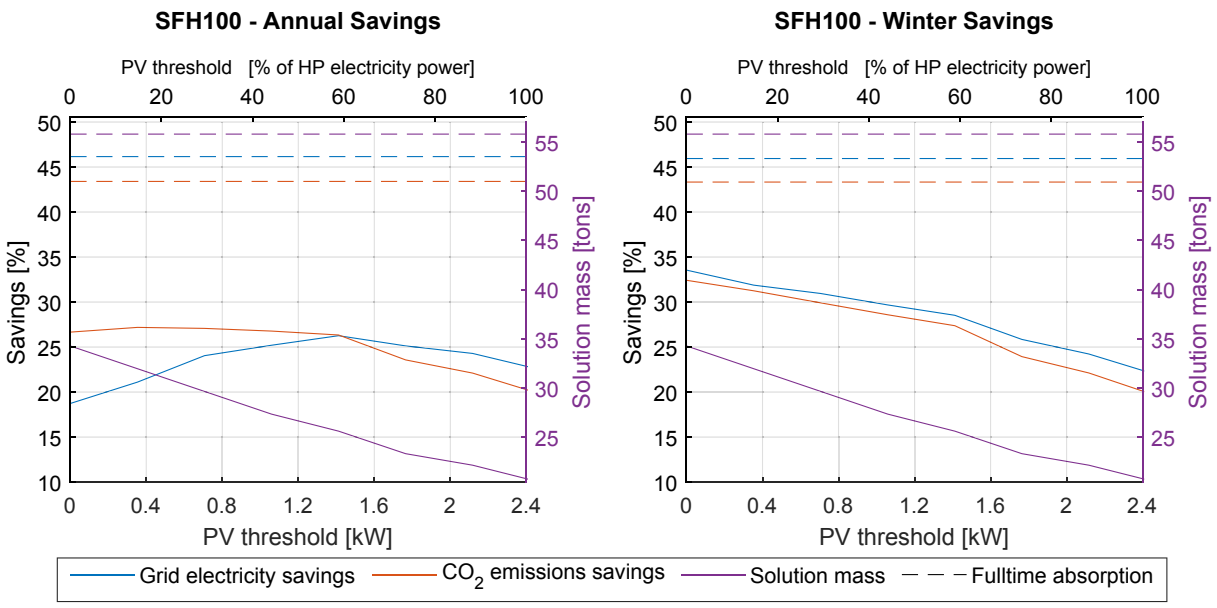

Fig. 9. SFH100 with ideal HP annual (left) and winter (right) grid electricity and CO_2 emission savings compared to reference system.

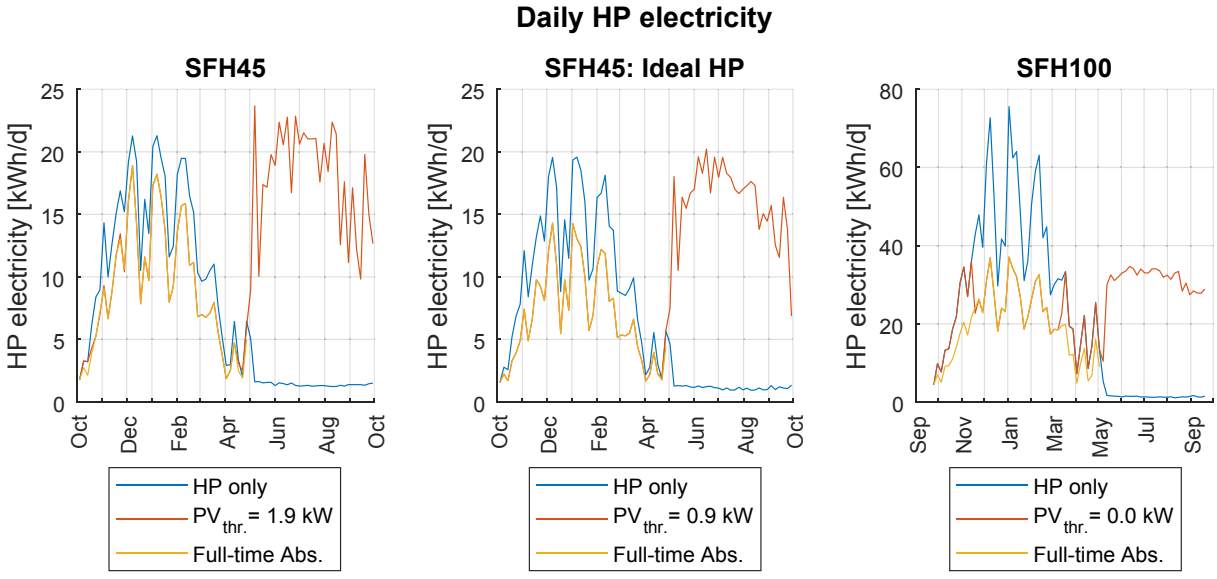

Fig. 10. Daily profiles of HP electricity consumption for SFH45 real HP (left), SFH45 with ideal HP (middle) and SFH100 (right).

negligible as the piping connecting the SR and the HP would be short in length.

3. Results and discussion

The duration and timing of the absorption period in winter were optimized for each building case. Each case is first simulated with infinite amount of available solution in the high concentration tank. This simulation will be referred to as "full-time absorption", as there is sufficient concentrated sorbent solution available for the sorption reactor to cover all heating loads during winter. From these simulations, the daily solution consumption and the solution concentration at the low concentration tank after the discharging period are calculated. The solution concentration is then used simulate the charging period to determine the actual available solution mass (50 wt%) for the coming winter.

The desorption process operates with the available PV electricity after the building's electricity loads are covered. The available electricity varies depending on the hour of the day and can be less or more than the electricity consumption of the heat pump (Table 2), leading to either partial, or full coverage of the desorption process electricity load. Therefore, several electricity thresholds for the start and the end of the desorption operation during the day were examined. For example, if the

$PV_{threshold}$ is set to 0 kW, the desorption process starts as soon as there is excess electricity in the early morning. The desorption process is then covered partially by the grid electricity and the locally produced renewable electricity, until the available PV electricity increases past the heat pump electricity power consumption. If the $PV_{threshold}$ is not reached the sorption reactor does not recharge the solution and the available PV electricity is fed to the grid.

The heat pump electricity consumption (maximum PV threshold) in desorption mode is determined by using the settings from Table 2 and the solution concentration in the low concentration tank after the full-time absorption simulation. The same threshold stops the charging mode in the evening. If the PV threshold is set equal to the heat pump's electricity load (indicated in Table 2), the sorption reactor operates entirely with renewable electricity. The lower this threshold is set, the more operating hours of the desorption process each day are achieved and, consequently, more solution can be regenerated; albeit with increasing fractions of grid electricity. The daily sorbent solution consumption from the "full-time absorption" simulations is then used in every $PV_{threshold}$ case to place the absorption period in the middle of the winter when the lowest ambient temperatures are encountered, and the impact of the absorption process is most beneficial. The various thresholds, respective regenerated solution mass and optimum absorption periods are given in Table 3. In the SFH45 cases the solution needed for the full-time absorption can be regenerated at multiple thresholds while in the SFH100 case, where the space heating demand is much larger, the charging period is not sufficient to regenerate the amount of solution required to cover the entire heating period.

Each building case was simulated with the absorption storage running under the different PV threshold settings as well as with full-time absorption and was compared to the reference system without sorption storage. The annual and winter results in terms of grid electricity and CO_2 emissions savings are given in Fig. 7 through Fig. 9 below.

Annual savings (Fig. 7 through Fig. 9, left figures) refer to actual grid electricity savings thus efficiency gain due to double staging the heat pump. On an annual basis, it does increase with increasing PV threshold because it lowers grid electricity demand of the heat pump in charging operation. In SFH45 with real HP (Fig. 7), when the critical PV threshold is exceeded such that the available solution mass starts decreasing, the annual savings (electricity and CO_2 emissions) stop increasing, stabilize and marginally decrease towards the highest threshold value. However, between the $PV_{thresholds}$ of 1.6 kW and 1.9 kW the electricity savings keep increasing even though the available solution has decreased, and absorption takes place less time during winter. This is because the grid electricity demand during charging reduces and outweighs the elevated HP electricity consumption in winter. When the $PV_{threshold}$ increases to 1.9 kW, less grid electricity is consumed during summer for charging. Consequently, less solution is available in winter for absorption, but since the absorption period is optimized to take place in the middle of the winter, the "lost" absorption hours correspond to early and late winter. During these days ambient temperatures remain high enough for the HP to achieve an adequately high COP in the reference case, thus reducing the beneficial effect of the SR. In the winter results (Fig. 7, right), all savings decrease as soon as the available solution reduces, since the charging period is not considered and the HP operates with a lower COP to cover the heating load when the SR does not operate.

With the ideal heat pump (Fig. 8), the decrease in winter electricity demand is larger (increased benefit of double staging because of the lower $T_{E,HTF,in}$ setting and constant isentropic efficiency) such that the maximum savings are achieved at lower PV thresholds compared to SFH45 with the real heat pump. Overall annual savings decrease again for further increase of PV threshold. For the SFH100 (Fig. 9), the available heat pump capacity is the limiting factor for regenerating enough sorbent solution during summer for subsequent winter operation. Consequently, solution mass continuously decreases with increasing PV threshold. Similarly, CO_2 emission savings almost monotonously decrease with increasing PV threshold, as winter electricity savings gradually decrease. The grid electricity savings in contrast first rise and then decrease again. Optimal PV threshold for annual electricity savings are 1.9 kW for SFH45 with the real heat pump, 1.2 with the ideal heat pump and 1.4 kW for the SFH100. For the CO_2 -savings optima are at 1.5, 0.9 and 0.3 kW. The difference in optimal PV thresholds for grid electricity and CO_2 emission savings respectively is due to the variable CO_2 intensities of grid electricity across seasons. Higher CO_2 intensities in winter lead to a shift towards lower optimal PV thresholds for CO_2 emission savings. This is most expressed for the SFH 100 where installed heat pump capacity is not sufficient for full absorption and thus low PV thresholds are necessary to significantly reduce winter electricity savings and thus CO_2 emissions.

In the best case, annual grid electricity/ CO_2 emission savings for SFH45 (Fig. 7, $PV_{threshold} = 1.9$ kW) reach around 37/34% for the real and 41/41% for the ideal heat pump (Fig. 8, $PV_{threshold} \sim 1.05$ kW). The ideal heat pump provides consistently high COPs at low temperature lifts, thus effectively benefiting from low condensation temperatures required in double stage configuration. For SFH100 (Fig. 9) the annual electricity and CO_2 emission savings are around 26% at $PV_{threshold} = 1.4$ kW. Here, the limiting factor is the available charging power of the heat pump. Theoretical savings, if charging power was unlimited and absorption could be run for the entire heating season, are around 46%, i.e. close to what could be reached for SFH45 with an ideal heat pump.

Winter savings (Fig. 7 through Fig. 9, right figures) are essentially expressing the load shift and the consequent increase in winter performance of the heat pump. Naturally, this does not depend on the PV threshold unless it is too high such that charging operation is insufficient, like for high PV thresholds in SFH45 cases (Fig. 7 and Fig. 8) or in the SFH100 (Fig. 9) case, where no PV threshold can regenerate enough solution mass. In the winter savings figures, there is just a very small offset between electricity and CO_2 emission savings for all building cases, as there is no difference in weighting of the CO_2 emission per kWh electricity use as there is across seasons. The winter electricity/ CO_2 emission savings for the SFH45 are around 34% and 42% for the real (Fig. 7, $PV_{threshold} = 1.6$ kW) and the ideal HP (Fig. 8, $PV_{threshold} = 0.9$ kW) respectively. Best case with zero PV threshold in SFH100 is around 34%, while the theoretical savings are approximately 45%.

In SFH100, winter savings are higher than all year savings (not the case for SFH45). This is because sorption capacity is dependent on the PV threshold chosen. When PV threshold is set to 0 to maximize storage capacity, grid electricity demand in summer will rise. When set above 0, sorption capacity will drop. Thus, maximum winter savings are encountered for zero PV threshold and lie above annual savings because summer grid demand is excluded. In SFH45, sorption capacity is sufficient to cover the entire winter period. Thus, PV threshold can be increased (without reducing storage capacity) while minimizing grid electricity demand in summer. For this reason, summer and winter savings are the same. A detailed result table is given in the appendix (Table A1).

When looking at the load profiles of the heat pump in Fig. 10, especially for the SFH45 ideal HP and SFH100, a significant seasonal load shift is visible from winter into summer. This shift expressed less for the SFH45 real HP case as the chosen commercial heat pump is not optimized for operation with low temperature lifts and is hence not able to exploit the available potential. For this reason, more attention is given the SFH45 ideal HP case as well as the SFH100 case where required temperature lifts better match the optimal performance range of the

commercial heat pump chosen. According to results represented in Table A1 the reduction in winter heat pump electricity demand and thus seasonal load shift for the SFH45 ideal is 743 kWh and for the SFH100 real it is 2542 kWh. This corresponds to relative savings of 33.5 and 33.3%. The winter grid electricity savings are 639 and 1993 kWh respectively. Compared to the reference case the latter corresponds to 42.3 and 33.5% savings in winter electricity demand from the electricity grid. This effect can also be seen when looking at the heat pump COPs and comparing them with the reference cases. For the SFH45 ideal, adding the sorption storage increases the heat pump winter COP from 3.63 to 5.47 and from 2.16 to 3.23 in the SFH100.

Besides electricity savings achieved through efficiency gains, it is crucial to see how this translates to CO_2 emission reductions. In contrast to electricity savings, where winter values are decisive, global emission reductions over the entire year should be considered. Difference to winter emissions is small(in the order of 5%), as in summer there is no space heating demand and most of DHW demand covered by PV without grid electricity support. For the SFH45 ideal heat pump case an annual CO_2 emission reduction of 108 kg is achieved corresponding to −40.3% compared to the reference. In SFH100 case 319 kg less are emitted, corresponding to a reduction of 29.8%.

Finally, the electricity savings achieved through storage integration need to be put in the context of renewable electricity production by the installed PV plant. Total annual PV production is 12′601 kWh contributing to the coverage of the annual household electricity (1′846 kWh) and the reference heat pump operation for space heating (2′388 SFH45 ideal and 7′807 SFH100). On an annual basis, the installed PV is thus sufficient to fully cover the total electricity demand even for the SFH100. On a real-time basis, this matching is of course not true because of the offset between maximum solar yield and maximum space heating demand. Taking the autarky or self-sufficiency level to express the fraction of total electricity demand covered with PV, 61.6 and 37.3% are achieved in the reference case for SFH45 ideal and SFH100 respectively. Including the load shifting capability provided through integration of the sorption storage, these values can both be increased to 83 and 56.3% respectively. Similarly, the self-consumption can be increased from 20.7 and 28.6% to 37.9 and 50.2% respectively. Because of the rather large PV system installed peak power in summer is too high to be fully exploited by the heat pump in charging operation such that a substantial amount of PV electricity needs to be fed back to the electricity grid thus leading to moderate self-consumption levels. It could be substantially increased by additionally installing an electric battery that would be able to be charged with high power.

Focusing on the thermal side, the heat demand covered with PV electricity can be expressed as a fraction of the total heat demand, defined as the solar fraction (SF). The solar fraction is thus increasing from the reference to the sorption storage case for the SFH45 ideal and SFH100 from 31.9 to 42.3% and from 23 to 22.5%. These numbers are achieved with priority of using available PV electricity to cover household electricity before covering heat pump electricity. If this priority is inverted, the SF can be increased in the SFH45 ideal case from reference 44% to 50.5% and in the SFH100 case from 30.4% to 28.4%. While in the SFH45 cases there is an increase of the SF, the SFH100 case shows the opposite result. The reason for this is the limited discharge power available from the sorption storage such that it needs to be operated not only during the day but also sometimes during the nights to cover the heating loads. During this extended operation there is an increased demand of grid electricity, explaining a reduction in the SF. Increasing discharge capacity of the sorption storage would be possible but it was found that it does not improve the overall electricity savings achieved. The non-linear modulation of the heat pump causes this result, as the electric consumption scales disproportionally to the heating power. The increase in the SF of SFH45 cases is also quite moderate. Again, the explanation can be found in the cap of the available absorber power, limiting the heat being produced in winter, while PV electricity is available. In the reference case, the available hp capacity is large enough to quickly charge the sensible buffer when PV electricity is available; heat pump operation after dusk can be stopped. With the sorption reactor, operation stretches beyond availability of PV. For the generation of heat, despite the efficiency increase achieved through the sorption storage, the electric heat pump still needs to be operated. This is in contrast to purely solar thermal systems, where thermal discharging is possible without heat pump operation and thus very low electricity demand. For rating the current system and system improvements, the autarky level is the more appropriate measure. The discussed results for the PV thresholds leading to highest CO_2 emission savings are achieved by the following storage dimensions:

In the SFH45 ideal case, sensible buffer storages of 1.8 m^3 (SH) and 0.2 m^3 (DHW) are used. Additionally, 20′300 kg 50 wt% concentrated sorbent solution (Fig. 8), 11′419 kg liquid water and consequently 31′719 diluted sorbent solution at an average of 32 wt% need to be stored. Assuming a density of the 50 wt% concentrated sorbent of 1′497 kg/m^3 at 60 °C and a density of the 32 wt% solution of 1′343 kg/m^3 at 30 °C and a density of water at 20 °C of 998 kg/m^3 a storage volume of 13.6 m^3, 23.6 m^3 and 11.4 m^3 respectively results.

In the SFH100 the mass of concentrated, diluted sorbent and water of 35′000, 54′688 and 19′688 kg are required, resulting in 23.4, 40.7 and 19.7 m^3 respectively. Additionally, water storages of 4 m^3 for space heating and 0.2 m3 for DHW are to be installed. The sorption storage requires storage of three species, i.e. concentrated and diluted sorbent solution as well as water. In any state of the storage, charged or discharged, there is a significant dead volume. With a flexible tank design (avoiding dead volume), the total storage size could be reduced to the volume of the diluted sorbent solution. This would significantly increase the achieved volumetric storage density when seen from a system perspective. With reference to the diluted sorbent volume (neglecting dead volume) the achieved volumetric energy density is 333.8 kWh/m^3 and 284.7 kWh/m^3 for the SFH45 ideal and SFH100 respectively.

3.1. Comparison to solar-assisted heat pump (SAHP) systems

The current study strives to minimize the electricity demand for space heating in winter by coupling a compression heat pump with a sorption process in a cascaded manner and to integrate renewables by means of AC solar photovoltaic system. There are many alternative system concepts with similar aims of fostering integration of renewables in buildings reported in literature. Under the name of solar-assisted heat pumps (SAHP), various combinations of classical compression heat pumps and solar harvesting technologies, such as solar thermal collectors, photovoltaic systems and hybrid photovoltaic/thermal collector systems (PV/T), are being researched with the aim of lowering the demand of primary energy for heat generation. Integration of solar heat with the compression cycle is either direct or indirect. In the direct integration case, the refrigerant is evaporated in the solar harvesting device directly, leading to typically higher efficiencies. Further differentiation is made by the type of heat pump being used, generally either air-source or ground-source heat pump. The latter has the benefit of a large thermal storage capacity being available, allowing for high heat pump performance also during winter.

In [49] a chronological review of solar-assisted heat pump research and development efforts in the 21st century is presented. In their review of research studies across all system types, the largest efficiencies are reported for direct expansion solar-assisted heat pumps (DX-SAHP), with COPs for space heating ranging from 5 to 7. In [50], solar

combinations with air-source heat pumps particularly are reviewed, with the conclusion that combinations with PV show highest thermo-economic potential. In [51], different SAHP approaches found in literature are presented by application types. For the space heating application, combinations of solar PV with air-source heat pumps energy savings of 22% and 35 % are reported by [52] and [53] respectively. In combination with ground source heat pumps energy savings between 14.5% and 32 % are reported by various authors.

Despite the significant importance of thermal energy storage in the coupling of solar with heat pumps not much attention is paid to this in these reviews. In the case of ground-coupled heat pump, an inherent storage capacity is part of the system concept and usually exploited by means of solar regeneration of the ground storage.

Other studies put more focus on the thermal energy storage and its long-term storage capability to achieve higher solar fractions in space heating operation. Among these, [54] featuring 40 m^2 of solar collectors and a 40 m^3 sensible water tank for a building with 240 m^2 floor area reports a 40% electricity demand reduction compared to the air-source heat pump system with short-term storage only. These savings are thus comparable to what the current study reports. Similarly, comparably high COPs are reported, by DX-SAHP or some ground-coupled SAHP system approaches. For a robust performance comparison of the different SAHP systems a detailed analysis of respective boundary conditions under which they have been evaluated would be required.

4. Summary and conclusions

A grey box model was built to realistically represent a liquid sorption storage and to study its building integration. A linear scaling factor was applied to match the charge and discharge power of the storage to the requirements of the building. As desorption power is the limiting factor determining the available storage capacity, a different scaling for charging and discharging operation was applied. This could be realized in a real system by operating different numbers of parallel heat exchangers.

The linear scaling approach chosen leads to overestimated thermal losses at larger scales of the storage. For this reason, the performance reported in this article may be considered a conservative estimate and better performance could be realistically expected.

Based on the derived sorption storage model, the integration of sorption storage in combination with an electric heat pump and rooftop photovoltaics (PV) has been studied. Real heat pump performance curves have been used in the simulations for two building cases (single family homes) SFH45 and SFH100. As the chosen real heat pumps are not optimized for low temperature lifts, their isentropic efficiency is relatively low in this operation domain. For this reason, an ideal heat pump has been additionally simulated in the SFH45 case to better exploit the efficiency potential available from double-staging and reducing the temperature lift provided by the heat pump.

For the SFH45, the achieved sorption storage capacity was large enough to cover full absorption during heating period; this was not achieved for SFH100. The latter building showed an excessive heat demand such that the available heat pump and sorption storage charging power was not sufficient to generate sorbent capacity.

Different PV thresholds have been explored to determine an optimal operation mode of the sorption storage minimizing over-all CO_2 emissions. The range of suitable PV thresholds in the SFH45 case indicated that the PV installation could be downsized without negative impact on the winter electricity savings. This is not true for SFH100 where all the PV is needed.

In all building cases simulated, the double-staging of the electric heat pump and the sorption storage led to an improved winter COP, an electric load shift from winter to summer and a commensurate CO_2 emission reduction. The performance improvements achieved can be considered significant –CO_2 emission reductions of up to 41% are recorded for the SFH45 ideal case.

The benefit of installing sorption storage may also be appreciated looking at the autarky or self-sufficiency levels achieved, reaching in the best case (SFH45 ideal) a value of 83%. Consequently, only 17% of the total electricity demand for household appliances, space heating and domestic hot water needs to be taken from the electric grid. Most important in this regard are the significant demand reduction of grid electricity in winter. Further optimizations in this direction could be achieved in combination with electric batteries. The latter would also allow for an eventual reduction of installed PV and the finding of an economic optimum of the entire installation.

In conclusion, combining electric heat pumps with a compact seasonal sorption storage largely contributes to the sectoral coupling between heat and electricity and the aim of achieving energy flexible buildings; being a necessary condition to better integrate fluctuating renewables into our energy system and thus driving its decarbonization.

CRediT authorship contribution statement

Efstratios Tzinnis: Data curation, Formal analysis, Investigation, Methodology, Software, Validation, Visualization, Writing - original draft, Writing - review & editing. **Luca Baldini:** Conceptualization, Funding acquisition, Investigation, Methodology, Project administration, Resources, Supervision, Validation, Writing - original draft, Writing - review & editing.

Declaration of Competing Interest

The authors declare that they have no known competing financial interests or personal relationships that could have appeared to influence the work reported in this paper.

Acknowledgements

This work was financially supported by the Swiss Innovation Agency Innosuisse in the frame of the Swiss Competence Centre for Energy Research Heat and Electricity Storage (SCCER HaE), grant Nr. 1155002545 and the Swiss Federal Office of Energy SFOE grant Nr. SI/501605-01.

Appendix

(See Figs. A1-A11)
(See Table A1)

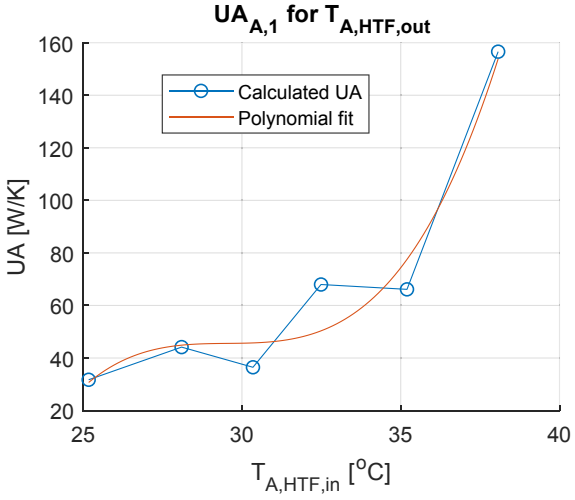

Fig. A1. Example of partial UA function: $UA_{A,1}$ at different $T_{A,htf,in}$.

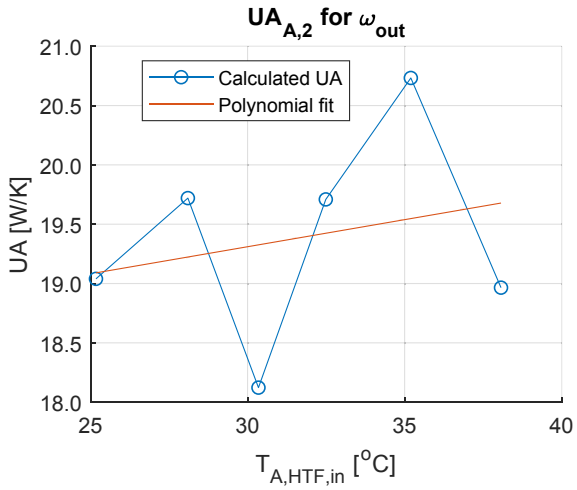

Fig. A2. Example of partial UA function:$UA_{A,2}$ at different $T_{A,htf,in}$.

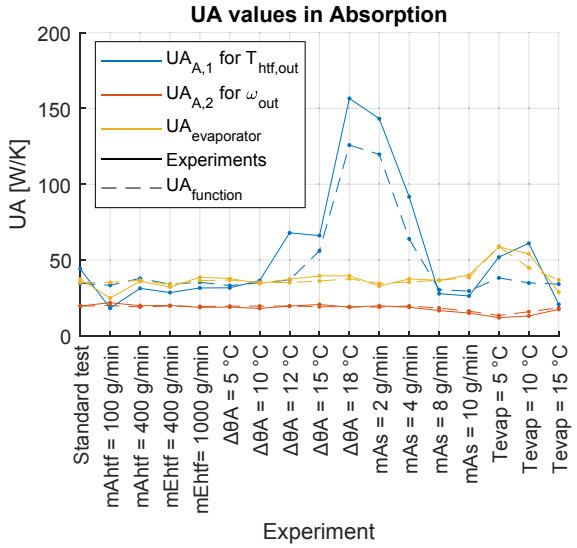

Fig. A3. Conformity of the derived UA functions (dashed) to the experimental values (solid) in absorption.

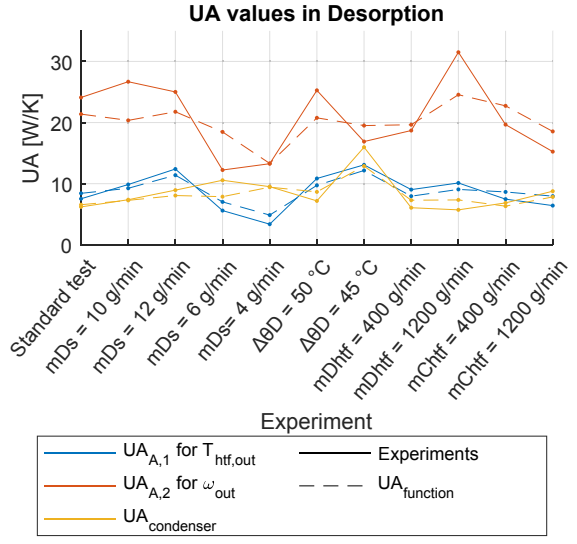

Fig. A4. Conformity of the derived UA functions (dashed) to the experimental values (solid) in desorption.

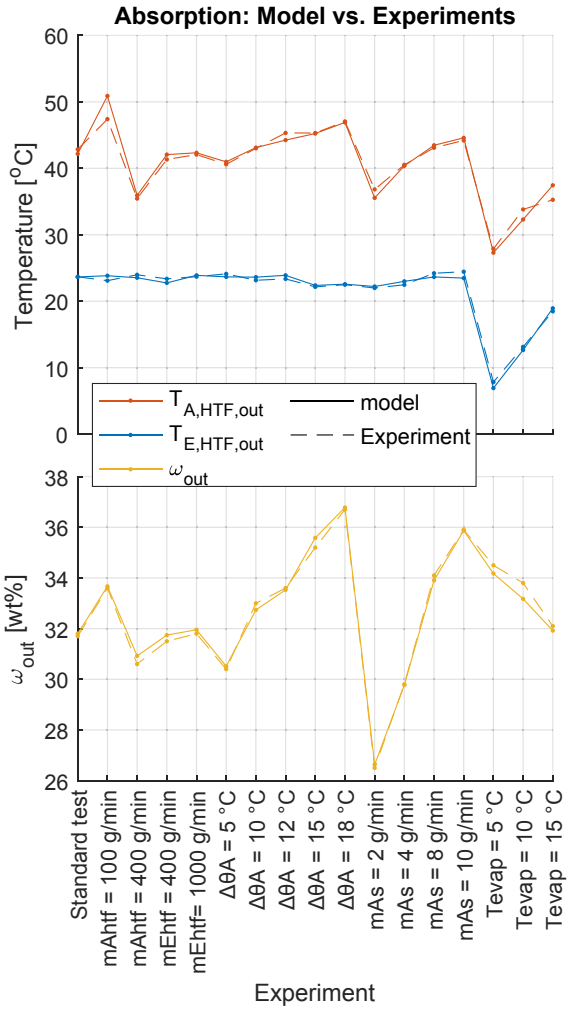

Fig. A5. Model results vs. experiments for absorption.

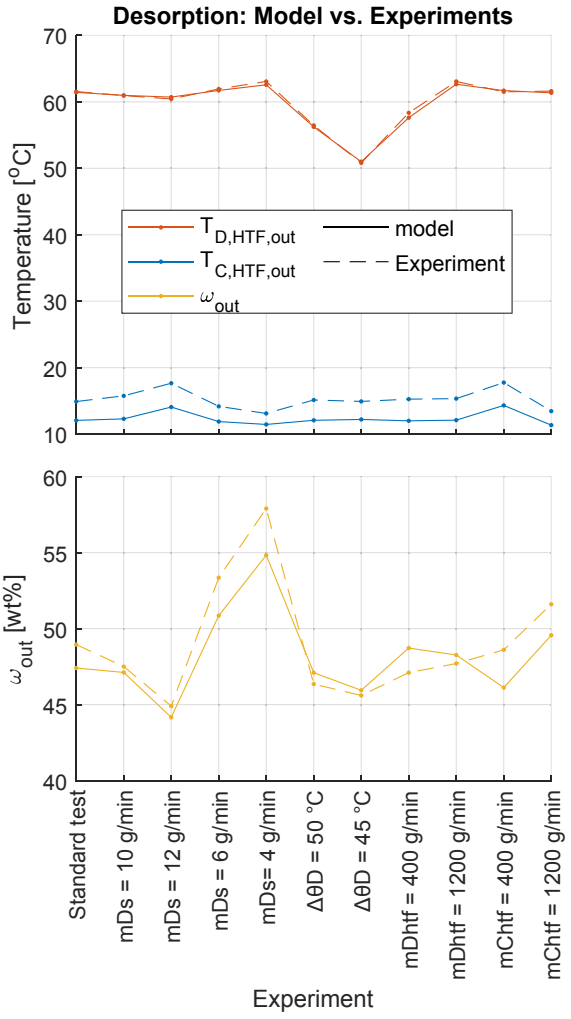

Fig. A6. Model results vs. experiment for desorption.

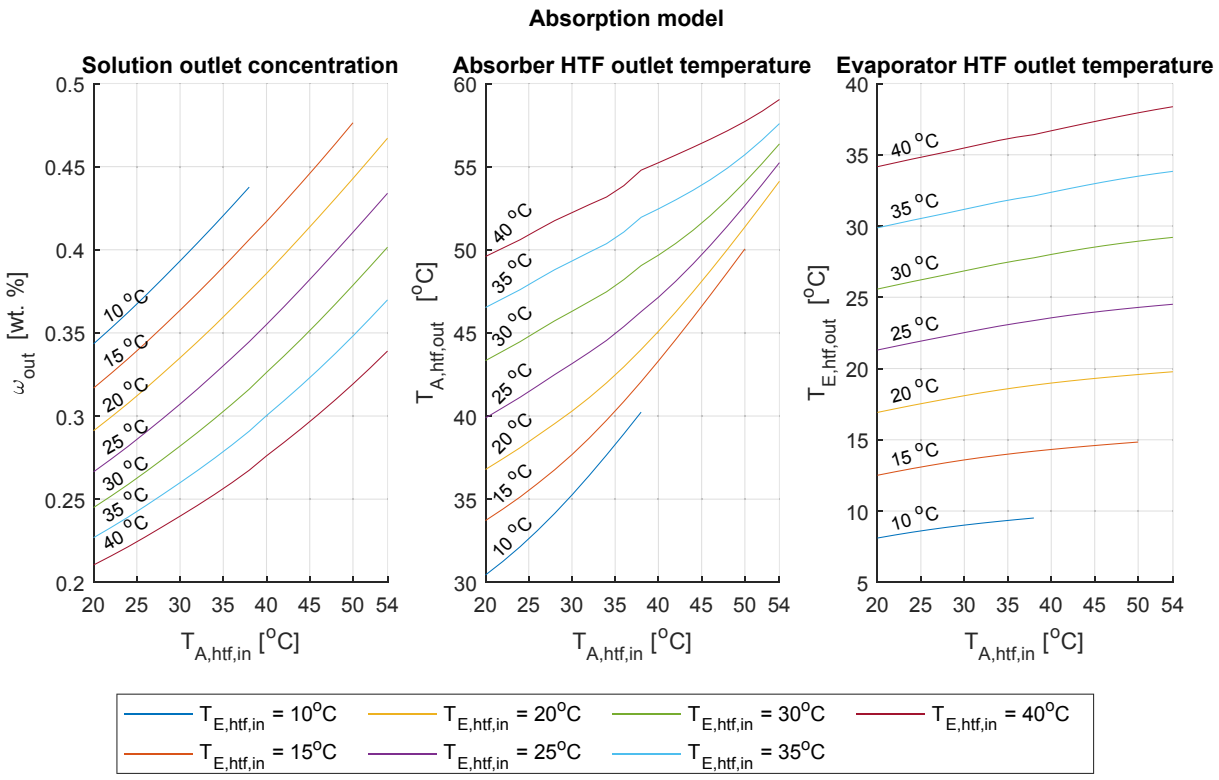

Fig. A7. Characteristic curves of sorption reactor model in absorption operation: ω_{out}, $T_{A,HTF,out}$, $T_{E,HTF,out}$.

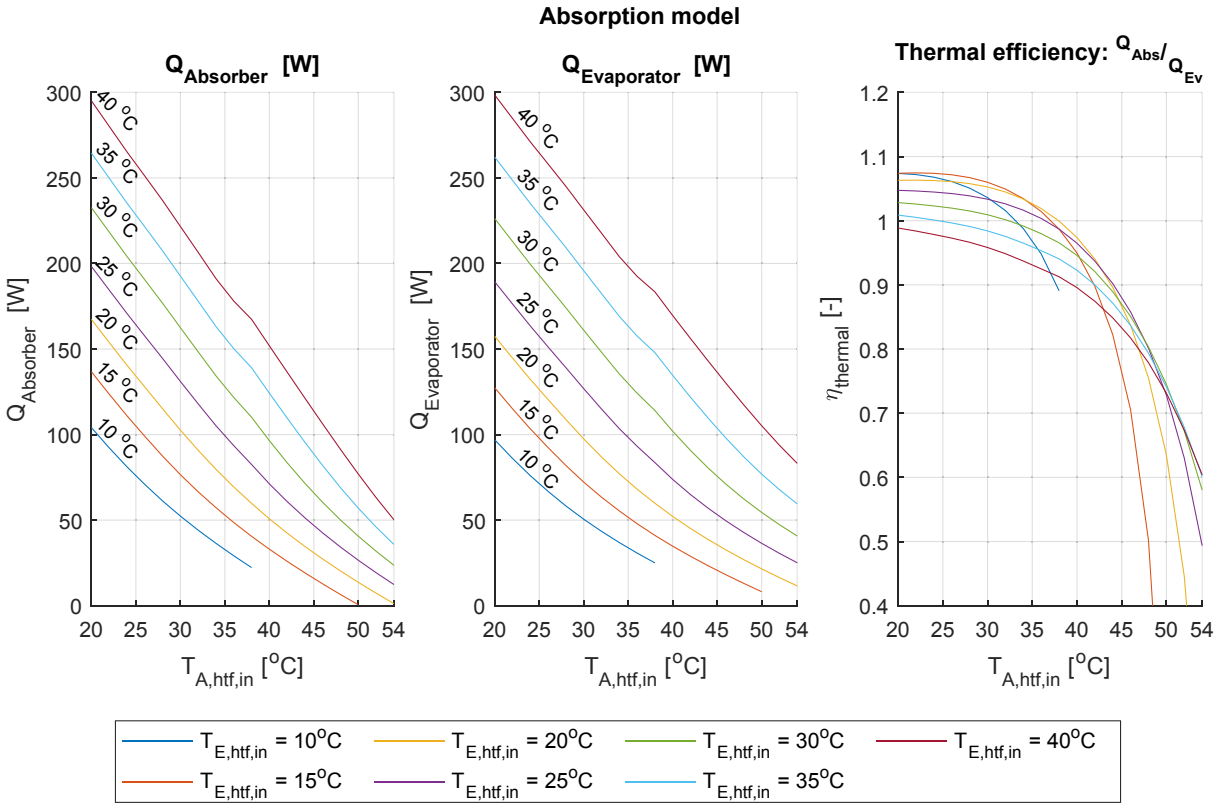

Fig. A8. Characteristic curves of sorption reactor model in absorption operation: Q_{Abs}, Q_{Ev}, thermal efficiency.

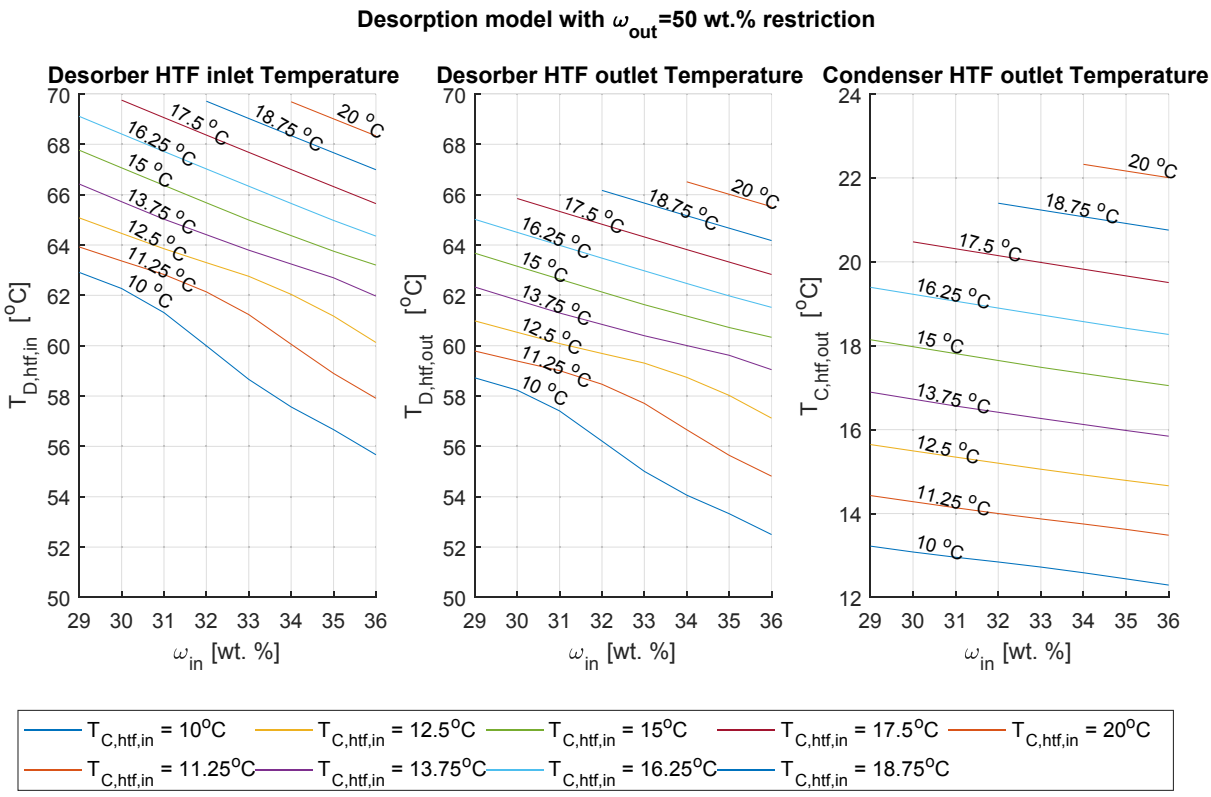

Fig. A9. Characteristic curves of sorption reactor model in desorption operation for full solution regeneration back to 50 wt%: $T_{D,HTF,in}$, $T_{D,HTF,ou}$, $T_{C,HTF,out}$.

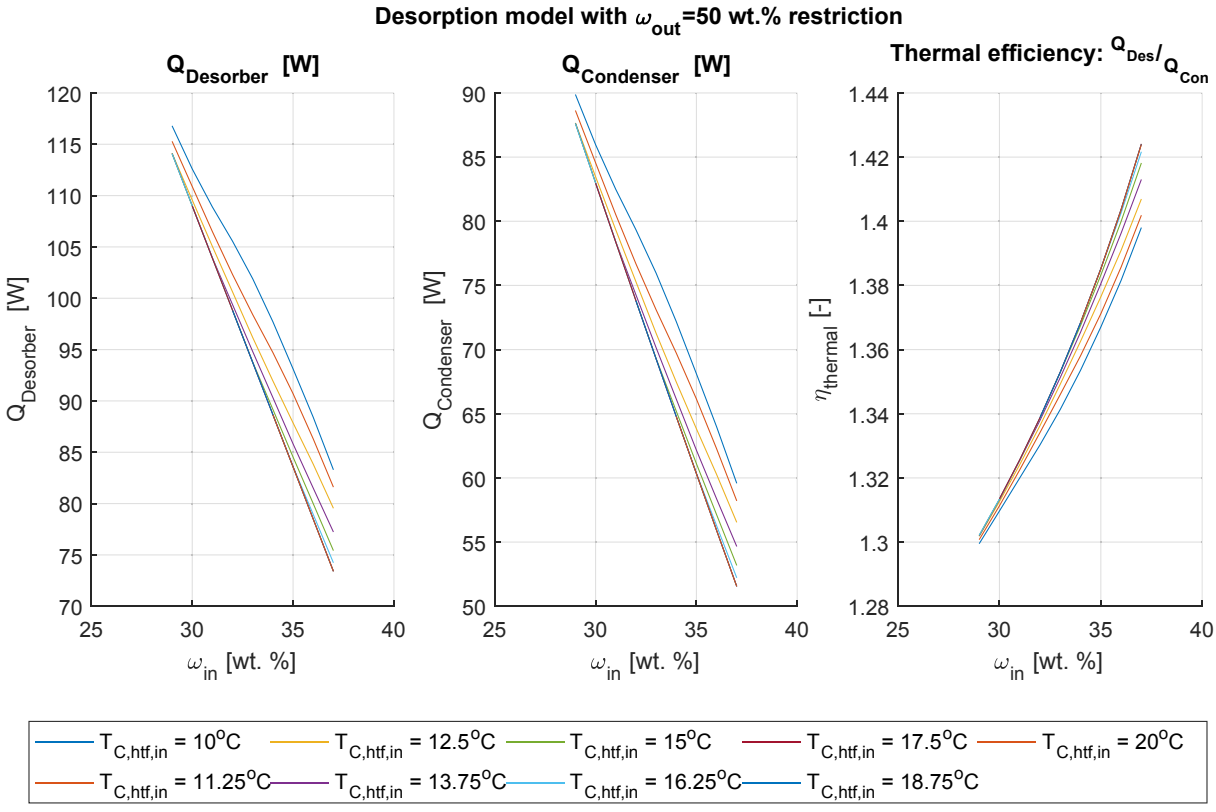

Fig. A10. Characteristic curves of sorption reactor model in desorption operation for full solution regeneration back to 50 wt%: Q_{Des}, Q_{Con}, thermal efficiency.

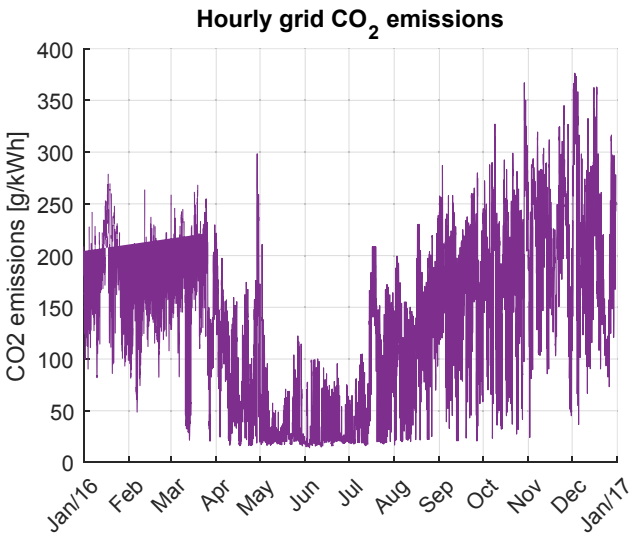

Fig. A11. CO_2 emissions [g/KWh$_{el}$] of the swiss electricity grid in 2016 taken from [46]. Hourly (left) and daily averaged (right) values.

Table A1
TRNSYS simulations results.

Simulations results		**SFH45**			**SFH45 Ideal HP**			**SFH100**		
		Reference	Optimum $PV_{thr.}$ 1.9 kW	Full-time absorption	Reference	Optimum $PV_{thr.}$ 0.9 kW	Full-time absorption	Reference	Optimum $PV_{thr.}$ 0 kW	Full-time absorption
SH load	[kWh]	6470						14,029		
DHW load	[kWh]	1968								
Building electricity	[kWh]	1846								
PV production	[kWh]	12,601								
HP electricity (winter)	[kWh]	2509	1924	1896	2219	1476	1464	7626	5084	4329
HP electricity	[kWh]	2717	4673	4488	2388	3917	3618	7807	9392	6890
Grid electricity (winter)	[kWh]	1587	1063	1041	1509	871	856	5942	3949	3212
Grid electricity	[kWh]	1738	1099	1074	1624	982	895	6048	4915	3256
Feed-in electricity	[kWh]	9776	7181	7341	9991	7820	8032	8996	6278	7121
CO_2 emissions	[kg]	291	192	188	268	160	153	1027	753	581
Solution Concentration	[wt. %]	–	31 – 50 wt%		–	33 – 50 wt%		–	34 – 50 wt%	
Solution mass @50 wt %	[tons]	0.0	15.6	16.6	0.00	20.1	20.6	0.00	34.3	55.8
Absorption period		–	18 Oct–18 Apr	10 Oct–26 Apr	–	16 Oct–20 Apr	10 Oct–26 Apr	–	02 Dec–28 Feb	29 Sep–03 May
winter COP		3.18	4.19	4.26	3.63	5.47	5.51	2.16	3.23	3.78
Grid electricity savings (winter)	[%]	0.0	33.0	34.4	0.0	42.3	43.3	0.0	33.5	45.9
Grid electricity savings	[%]	0.0	36.7	38.2	0.0	39.5	44.9	0.0	18.7	46.2
CO_2 emissions savings (winter)	[%]	0.0	32.1	33.5	0.0	41.6	42.1	0.0	32.4	43.3
CO_2 emissions savings	[%]	0.0	34.0	35.3	0.0	40.6	42.9	0.0	26.7	43.4
Autarky	[%]	61.9	83.1	83.0	61.6	83.0	83.6	37.3	56.3	62.7
self-consumption	[%]	22.4	43.0	41.7	20.7	37.9	36.3	28.6	50.2	50.1
Heating solar fraction	[%]	36.5	47.4	47.8	31.9	42.3	42.9	23.0	22.5	28.0
SR discharged heat	[kWh]	–	7679	8005	–	7818	8000	–	11,588	16,271

References

[1] Agreement P. Paris agreement. In: Report of the Conference of the Parties to the United Nations Framework Convention on Climate Change (21st Session, 2015: Paris). Retrieved December; 2015, vol. 4: HeinOnline, p. 2017.

[2] European Heat Pump Market and Statistics Report 2019. September 2019; 2019.

[3] Baldini L, Fumey B. Seasonal Energy Flexibility Through Integration of Liquid Sorption Storage in Buildings. Energies 2020;13(11):2944. https://doi.org/10.3390/en13112944.

[4] Hadorn JC. Thermal energy storage for solar and low energy buildings: State of the art by the solar heating and cooling task SHC 32. Universidad de Lleida 2005.

[5] N'Tsoukpoe KE, Liu H, Le Pierrès N, Luo L. A review on long-term sorption solar energy storage. Renew Sustain Energy Rev 2009;13(9):2385–96. https://doi.org/10.1016/j.rser.2009.05.008.

[6] Ding Y, Riffat SB. Thermochemical energy storage technologies for building applications: a state-of-the-art review. Int J Low-Carbon Technol 2013;8(2):106–16. https://doi.org/10.1093/ijlct/cts004.

[7] Tatsidjodoung P, Le Pierrès N, Luo L. A review of potential materials for thermal energy storage in building applications. Renew Sustain Energy Rev 2013;18:327–49. https://doi.org/10.1016/j.rser.2012.10.025.

[8] Xu J, Wang RZ, Li Y. A review of available technologies for seasonal thermal energy storage. Solar Energy 2014;103:610–38. https://doi.org/10.1016/j.solener.2013.06.006.

[9] Heier J, Bales C, Martin V. Combining thermal energy storage with buildings – a review. Renew Sustain Energy Rev 2015;42:1305–25. https://doi.org/10.1016/j.rser.2014.11.031.
[10] Solé A, Martorell I, Cabeza LF. State of the art on gas–solid thermochemical energy storage systems and reactors for building applications. Renew Sustain Energy Rev 2015;47:386–98. https://doi.org/10.1016/j.rser.2015.03.077.
[11] Scapino L, Zondag HA, Van Bael J, Diriken J, Rindt CCM. Sorption heat storage for long-term low-temperature applications: A review on the advancements at material and prototype scale. Appl Energy 2017;190:920–48. https://doi.org/10.1016/j.apenergy.2016.12.148.
[12] Krese G, Koželj R, Butala V, Stritih U. Thermochemical seasonal solar energy storage for heating and cooling of buildings. Energy Build 2018;164:239–53. https://doi.org/10.1016/j.enbuild.2017.12.057.
[13] Kuznik F, Johannes K, Obrecht C, David D. A review on recent developments in physisorption thermal energy storage for building applications. Renew Sustain Energy Rev 2018;94:576–86. https://doi.org/10.1016/j.rser.2018.06.038.
[14] Fumey B, Weber R, Baldini L. Sorption based long-term thermal energy storage – Process classification and analysis of performance limitations: A review. Renew Sustain Energy Rev 2019/09/01/ 2019,;111:57–74. https://doi.org/10.1016/j.rser.2019.05.006.
[15] Tatsidjodoung P, Le Pierrès N, Heintz J, Lagre D, Luo L, Durier F. Experimental and numerical investigations of a zeolite 13X/water reactor for solar heat storage in buildings. Energy Convers. Manage. 2016;108:488–500. https://doi.org/10.1016/j.enconman.2015.11.011.
[16] Köll R, van Helden W, Engel G, Wagner W, Dang B, Jänchen J, et al. An experimental investigation of a realistic-scale seasonal solar adsorption storage system for buildings. Sol Energy 2017;155:388–97. https://doi.org/10.1016/j.solener.2017.06.043.
[17] Jaehnig D. Simulation Report System: Closed-Cycle Sorption Storage "MODESTORE"; 2008.
[18] Kerskes H, Asenbeck S. Simulation Report System: Monosorp; 2008.
[19]] Zondag H. Simulation report System: ECN TCM model; 2008.
[20] Engel G, Asenbeck S, Köll R, Kerskes H, Wagner W, van Helden W. Simulation of a seasonal, solar-driven sorption storage heating system. J Storage Mater 2017;13:40–7. https://doi.org/10.1016/j.est.2017.06.001.
[21] Weber R, Fumey B, Moser C, Baldini L. TRNSYS simulation of a sodium hydroxide sorption storage system. presented at the SOLARIS Conference 2017, Brunel University, London, July 27/28, 2017. 2017.
[22] Mlakar U, Stropnik R, Koželj R, Medved S, Stritih U. Experimental and numerical analysis of seasonal solar-energy storage in buildings. Int J Energy Res 2019;43(12):6409–18. https://doi.org/10.1002/er.v43.1210.1002/er.4449.
[23] Hennaut S, Thomas S, Davin E, André P. Dynamic simulation of residential buildings with seasonal sorption storage of solar energy-parametric analysis. In: 30th ISES Biennial Solar World Congress 2011, SWC 2011; 2011. p. 4686–95.
[24] Frazzica A, Brancato V, Dawoud B. Unified methodology to identify the potential application of seasonal sorption storage technology. Energies 2020;13(5):1037. https://www.mdpi.com/1996-1073/13/5/1037.
[25] Stitou D, Mazet N, Mauran S. Experimental investigation of a solid/gas thermochemical storage process for solar air-conditioning. Energy 2012;41(1):261–70. https://doi.org/10.1016/j.energy.2011.07.029.
[26] Chen Y, Desai A, Schmidt F, Xu P. Electricity demand flexibility performance of a sorption-assisted water storage on building heating. Appl Therm Eng 2019;156:640–52. https://doi.org/10.1016/j.applthermaleng.2019.04.080.
[27] Aydin D, Casey SP, Chen X, Riffat S. Numerical and experimental analysis of a novel heat pump driven sorption storage heater. Appl Energy 2018;211:954–74. https://doi.org/10.1016/j.apenergy.2017.11.102.
[28] Finck C, Li R, Kramer R, Zeiler W. Quantifying demand flexibility of power-to-heat and thermal energy storage in the control of building heating systems. Appl Energy 2018;209:409–25. https://doi.org/10.1016/j.apenergy.2017.11.036.
[29] Arteconi A, Hewitt NJ, Polonara F. Domestic demand-side management (DSM): Role of heat pumps and thermal energy storage (TES) systems. Appl Therm Eng 2013;51(1):155–65. https://doi.org/10.1016/j.applthermaleng.2012.09.023.
[30] Arteconi A, Polonara F. Assessing the demand side management potential and the energy flexibility of heat pumps in buildings. Energies 2018;11(7). https://doi.org/10.3390/en11071846.
[31] Fumey B, Weber R, Baldini L. "Liquid sorption heat storage – a proof of concept based on lab measurements with a novel spiral fined heat and mass exchanger design," (in eng). Appl Energy 2017;200:215–25. https://doi.org/10.1016/j.apenergy.2017.05.056.
[32] Scapino L, Zondag HA, Diriken J, Rindt CCM, Van Bael J, Sciacovelli A. Modeling the performance of a sorption thermal energy storage reactor using artificial neural networks. Appl Energy 2019;253:113525. https://doi.org/10.1016/j.apenergy.2019.113525.
[33] Palomba V, Dino GE, Frazzica A. Coupling sorption and compression chillers in hybrid cascade layout for efficient exploitation of renewables: Sizing, design and optimization. Renew. Energy 2020;154:11–28. https://doi.org/10.1016/j.renene.2020.02.113.
[34] Morawetz E. Sorption-compression heat pumps. Int J Energy Res 1989;13(1):83–102. https://doi.org/10.1002/(ISSN)1099-114X10.1002/er.v13:110.1002/er.4440130109.
[35] Gado MG, Ookawara S, Nada S, El-Sharkawy II. Hybrid sorption-vapor compression cooling systems: A comprehensive overview. Renew Sustain Energy Rev 2021;143:110912. https://doi.org/10.1016/j.rser.2021.110912.
[36] Wu W, Wang B, Shi W, Li X. Absorption heating technologies: A review and perspective. Appl Energy 2014;130:51–71. https://doi.org/10.1016/j.apenergy.2014.05.027.
[37] Palomba V, Varvagiannis E, Karellas S, Frazzica A. Hybrid adsorption-compression systems for air conditioning in efficient buildings: design through validated dynamic models. Energies 2019;12(6):1161. https://www.mdpi.com/1996-1073/12/6/1161.
[38] Wu W, You T, Wang J, Wang B, Shi W, Li X, A novel internally hybrid absorption-compression heat pump for performance improvement; 2018.
[39] Energy IS. Mapping the Road Ahead. IEA: Paris, France; 2019.
[40] Olsson J, Jernqvist Å, Aly G. Thermophysical properties of aqueous NaOH−H2O solutions at high concentrations. Int J Thermophys 1997;18(3):779–93. https://doi.org/10.1007/bf02575133.
[41] Dott R, Haller M, Ruschenburg J, Ochs F, Bony J. The Reference Framework for System Simulations of the IEA SHC Task 44 / HPP Annex 38 Part A: General Simulation Boundary Conditions. Int Energy Agency 2013.
[42] Dott R, Haller M, Ruschenburg J, Ochs F, Bony J. The Reference Framework for System Simulations of the IEA SHC Task 44 / HPP Annex 38 Part B: Buildings and Space Heat Load. Int Energy Agency 2014.
[43] DesignBuilder Software. "DesignBuilder Dynamic Simulation Model (DSM) User Manual v5.4." https://designbuilder.co.uk. [Accessed: June 4, 2020].
[44] Vela Solaris AG, "Polysun User Manual," 2018. Accessed: June 4, 2020. [Online]. Available: https://www.velasolaris.com.
[45] Sunpower Maxeon 3 | 400 W, 2019. [Online]. Available: https://sunpower.maxeon.com/uk/. [Accessed: 30/04/2020].
[46] electricitymap.org. "CO_2 emissions of electricity consumption." https://www.electricitymap.org/map. [Accessed: April 30, 2020].
[47] Solar Energy Laboratory - University of Wisconsin-Madison. "TRNSYS 17 Software." https://sel.me.wisc.edu/trnsys/index.html. [Accessed: June 4, 2020].
[48] Hovalpartners. "UltraSource T comfort (8 - 17)." https://www.hoval.ch/de_CH/. [Accessed: January 4, 2021].
[49] Badiei A, et al. A chronological review of advances in solar assisted heat pump technology in 21st century. Renew Sustain Energy Rev 2020;132. https://doi.org/10.1016/j.rser.2020.110132.
[50] Wang Xinru, Xia Liang, Bales Chris, Zhang Xingxing, Copertaro Benedetta, Pan Song, et al. A systematic review of recent air source heat pump (ASHP) systems assisted by solar thermal, photovoltaic and photovoltaic/thermal sources. Renew Energy 2020;146:2472–87. https://doi.org/10.1016/j.renene.2019.08.096.
[51] Mohanraj M, Belyayev Y, Jayaraj S, Kaltayev A. Research and developments on solar assisted compression heat pump systems – A comprehensive review (Part-B: Applications). Renew Sustain Energy Rev 2018;83:124–55. https://doi.org/10.1016/j.rser.2017.08.086.
[52] Niederhäuser Elena-Lavinia, Huguelet Nicolas, Rouge Matthias, Guiol Pierre, Orlando David. Novel approach for heating/cooling systems for buildings based on photovoltaic-heat pump: concept and evaluation. Energy Procedia 2015;70:480–5.
[53] Wang C, Gong G, Su H, Wah Yu C. Efficacy of integrated photovoltaics-air source heat pump systems for application in Central-south China. Renew Sustain Energy Rev 2015;49:1190–7. https://doi.org/10.1016/j.rser.2015.04.172.
[54] Lu J, He G, Mao F. Solar seasonal thermal energy storage for space heating in residential buildings: Optimization and comparison with an air-source heat pump. Energy Sources Part B 2020;15(5):279–96. https://doi.org/10.1080/15567249.2020.1786192.